Chapter 2: Supports

2.1: Introduction

The steam, and dry/bi-reforming of hydrocarbons to produce syngas (a mixture of Carbon Monoxide and Hydrogen) are industrially important processes. They produce Syngas which is further used to produce methanol or liquid hydrocarbons by the Fischer-Tropsch process or oxoalcohols by hydroformylation. Hydrogen is an important source of energy. It is also used as a reactant for producing ammonia (food), cyclohexane (solvent), hydrodesulfurization, hydrodenitrification, hydrodemetallation (clean fuels) and for the valorization of atmospheric and vacuum residue by upgrading them through hydrocracking.

Catalytic steam reforming was commercialized about a century ago (around 1928). BASF was the pioneer who patented a nickel-based catalyst [1] for this application. Significant research and commercial modifications have been made since. SMR is a mature technology from a catalyst standpoint. Current R&D efforts are directed towards developing structured catalysts CATACEL SSR^{TM} – Johnson Matthey [2] or EARTH ® (Enhanced Annular Reforming Tube for Hydrogen) [51].

With the drive to Net Zero emission of CO_2, the focus on dry reforming and steam reforming of renewable feedstock has gained momentum. Catalysts which are used for Steam reforming are multicomponent (irrespective of the feedstock). They operate at high temperatures, low to moderate pressure as dictated by thermodynamics, and high space velocities. These catalysts need to have tolerance to the presence of moisture in the feed. The source of the moisture is steam which is co-fed along with the hydrocarbon as co-reactant. It also retards coke formation or oxygenates such as methanol or ethanol which are used as feedstock. Desirable attributes are adequate microstructure (moderate surface area and pore volume), resistance to hydrothermal sintering (loss of surface area/pore volume or mechanical strength of the support and minimum agglomeration of active metal particles), oxygen mobility (which is also referred to as OSC – Oxygen storage capacity for combustion/gasification of carbonaceous deposits), good mechanical and hydrothermal stability (resistance to changes in phases of metal oxides which constitute the support).

Such diverse attributes are rarely found in a single-component catalyst material, because of which it is necessary to formulate multicomponent (composites/supports/carriers) for this application.

A variety of materials viz. monocomponent alumina [3,4], magnesia [5,6,7], ceria [7,8,9,10], zirconia [11,12,13], Lanthana [14] have been reported in the literature. These are from Group IIIA, IIA, IVA and lanthanides from Group VA from the old periodic table.

Also studied are binary composites such as alumina promoted with either rare earth [15,16,17,18,19,20,21,22] or magnesia [22,23] or ZrO_2 [22]. Bicomponent materials such as Layered double hydroxides (LDH) [23] such as Al-Mg or Zn-Mg, a combination of either ceria-zirconia [24,25,26] or yttria-zirconia [27], or RE (rare earth) modified zirconia [28], or alumina-zirconia [29] have also been studied. Amongst ternary composites, materials such as RE-modified magnesium aluminate [30] or ceria-zirconia-alumina [21] or strontium-alumina-zirconia [31] are reported in literature either as carriers or as promoters for this application.

Various functions are attributed to Lanthana. It is reported to impart thermal stability [15,21], enhance nickel dispersion [18,19] and suppress the formation of nickel aluminate [15] phase which is difficult to reduce. However, it is also reported to decrease the specific surface area of the catalyst [16]. The scavenging of coke is an important function in steam reforming catalysts. OSC (oxygen storage capacity or oxygen mobility) is the ability of certain oxide materials to store oxygen in their lattice. The lattice oxygen is used in scavenging of coke deposits on the catalyst thus slowing catalyst deactivation. Two such materials are Ceria [17,21] and Lanthana oxycarbonate [15,17,18,28] which are reported to improve the stability of the catalyst by scavenging coke through mobile lattice oxygen. The drawback of Ceria (Ce) [17] and Lanthana (La) [22] which is reported, is the decrease in the activity of the catalyst due to the surface coverage of nickel [17,22] by these oxides when the catalyst is prepared by metal impregnation. Magnesium is reported to form its aluminate with alumina. This is reported to suppress the formation of nickel aluminate [22] because of which reducibility of Nickel oxide increases which in turn increases activity. Ternary Sr-Al_2O_3-ZrO_2 aerogel is reported to improve performance [31]. Zirconia-rich supports are reported less active [8]. Ceria-zirconia improves the dispersion of Nickel (Ni) [26]. Layered Double Hydroxide supports show high stability and decrease coke laydown

[23]. Zirconia (Zr) enhances the oxygen storage capacity of ceria as well as thermal stability through solid solution formation [24].

To summarize, most of the above examples are either monocomponent or bi-component materials. The results of the above studies show that each of these promoter elements imparts specific characteristics to the catalyst, and all these properties are important to the application of steam reforming.

Three major methods of catalyst preparation are reported in the literature. These are either Sol-gel [3.5.10.15.28.29.31], (co)-precipitation [6,8,9,14,26], or impregnation [3,4,5,6,7,8,9,10,12,13,15,16,19,21,22,24,25,26,30]. Of these the former two are rarely used for incorporating the active elements such as noble metals or Ni, Co. These are mainly used for preparing the alumina or magnesia supports and incorporating promoters such as La, Ce, Zr or Sr. Impregnation appears to be the preferred method for introducing promoters as well as the active metals because a large number of references report this method. When impregnation is used as the preparation technique for introducing promoters a variety of effects is reported. These are the surface coverage of nickel with lanthana [22], ceria and zirconia [21], as well as the formation of NiO-CeO_2 solid solution [17], segregation of CeO_2 [21,20] etc. Thus, in such cases (when impregnation is used as the method of preparation), an adverse effect on activity is reported. Co-precipitation is reported to result in a high degree of compositional homogeneity [8,15] whereas inhomogeneity of composition is reported when catalysts are prepared by impregnation [21].

The following examples reported in the literature serve as evidence for interaction effects between individual components of the carrier/promoter. Ni/Magnesia prepared by precipitation inhibits catalyst activity adversely due to formation of solid solution which retard the reduction of NiO [6]. Ni catalysts prepared by impregnation on support wherein Magnesia (Mg) is impregnated on alumina show high activity [22]. It is reported that this inhibits the formation of $NiAl_2O_4$ [22] which otherwise forms in alumina supports [29]. The formation of $NiAl_2O_4$ affects the reduction of nickel oxide to metallic Ni. La_2O_3/Al_2O_3 is reported to behave similarly [15] and facilitates ease of reduction of Ni oxide. Sintering of Ni and coke laydown is reported in Ni/CeO_2 [7], whereas promotion with zirconia improves dispersion and activity at high CeO_2 content [8]. Ni/ZrO_2 is reported to give high yields of H_2 and stability [13] whereas ZrO_2-rich Ceria-zirconia supports show low activity [8].

Thus, as seen from studies reported in the literature, a study of binary, ternary and quaternary supports which are prepared by co-precipitation is expected to add to the body of knowledge reported in published literature. There are only a few studies of ternary [21,30,31,38] supported catalysts reported in published literature, barring examples in patents that do not disclose structure-activity correlations and the reasons for the same. Similarly, there are no studies of Ni supported on quaternary carriers for the reforming of ethanol or natural gas in the existing literature.

In this work, a set of thirteen compositions/formulations of catalyst support covering three binary, seven ternary and three quaternary composites are prepared by co-precipitation and studied. The supports are also referred to as composites in the current study because they contain more than one metal oxide.

These supports constitute the following: Magnesia, alumina and zirconia form the primary constituents of the binary supports.

All the catalysts contain Rare Earth (La and Ce) as oxides. The concentration of these two oxides is fixed at a nominal value of 5.4 wt% each.

Combinations of alumina and magnesia or alumina and zirconia or magnesia and zirconia form the ternary supports. The composition of ternary catalysts is described as a 'Balanced' composition when both the components are present in equal concentrations expressed as weight%. The composition of ternary catalysts is described as 'Skewed' compositions when part of the alumina in catalysts with balanced composition is substituted either by magnesia or zirconia, depending on the composition. Only one catalyst with a balanced composition of Magnesia and Zirconia is prepared for this study.

Catalysts of quaternary composition are those in which the concentration of oxides of one of Al, Mg or Zr is higher than that of the other two. These other two have the same concentration by weight% in the catalyst.

The catalysts using the above carriers are studied for steam reforming of ethanol and also for the dry reforming of ethanol with nickel as the active metal. The Nickel is impregnated on these supports by incipient wetness method. The use of a common set of raw materials and preparation procedures enables the determination of interaction / synergistic effects between the components in an unbiased manner.

Composites are thoroughly characterized using a variety of techniques.

- Nitrogen (N_2) physisorption for microstructure (specific surface area, pore volume and pore size)
- Ammonia Temperature programmed Desorption (NH_3-TPD) to determine acidity and acid strength.
- The decomposition of C5 alcohol to assess acidic, amphoteric, and basic sites.
- Powder-XRD to determine metal oxide phase and crystallite size and changes in phase and crystallite size after hydrothermal aging.
- Fourier Transform Infrared Spectroscopy (FTIR) to identify hydroxide/oxide species in the supports.
- Differential Scanning Calorimetry-Thermal Gravimetric (DSC-TG) analysis to identify interaction effects between individual components of the supports.
- Oxygen storage capacity (OSC) to measure the storage of lattice oxygen.

These techniques helped to identify synergistic or interaction effects between the individual components of the support. Further, the composition space of the catalyst is correlated with these properties. The properties of these composites and their performance for ESR (Ethanol steam reforming – chapter 4) and EDR (Ethanol dry reforming – chapter 5) indicate that they are useful as catalyst carriers for dry and steam-reforming applications.

2.2: Experimental

2.2.1: Materials

Metal nitrates are used as the precursor salts because they decompose to the corresponding oxide without leaving behind any residue in the catalyst. Specific metal precursor salts used for catalyst preparation are $Al(NO_3)_3.9H_2O$ (CAS 7784-27-2), $Mg(NO_3)_2.6H_2O$ (CAS 7784-27-2), $La(NO_3)_3.6H_2O$ (CAS 10277-43-7), $Ce(NO_3)_3.6H_2O$ (CAS 10294-41-4) which are sourced from SD Fine Chemicals. $ZrO(NO_3)_2.xH_2O$ (CAS 4985-18-3) and NaOH (CAS 1310-73-2) which are sourced from Sigma Aldrich.

2.2.2: Preparation of supports

As described above in the introduction section, three binary supports, seven ternary supports and three quaternary supports are prepared. The content of Rare Earth

compounds, Lanthana and Ceria, is fixed at nominal 5.4wt% each in all the catalyst supports.

The supports are coded as AMZ-#-@-$, wherein #, @ and $ represent weight% of alumina, magnesia, and zirconia respectively. The concentration of ceria and lanthana are not included because they are at a nominal 5.4wt% each in all the catalysts.

The binary alumina catalyst (AMZ-89-0-0) consists of about 89wt% alumina with nominal 5.4wt% each of lanthana and ceria. Similarly, the magnesia (AMZ-0-89-0) and zirconia (AMZ-0-0-89) binary catalysts have 89% of these respective components in place of alumina.

The ternary supports consist of any two of alumina, magnesia, and zirconia (along with lanthana and ceria at nominal 5.4 wt% each). They are coded AMZ-44-44-0 (alumina-magnesia), AMZ-44-0-44 (alumina-zirconia), and AMZ-0-44-44 (magnesia-zirconia). These catalysts are referred to as ternary catalysts with balanced composition because the concentrations of the two major components expressed as weight% are the same. Ternary catalysts with skewed composition are also prepared and studied. These are coded AMZ-39-49-0 and AMZ-29-59-0 for the alumina-magnesia ternary catalysts where part of the alumina in the balanced catalyst composition is partially substituted with magnesia. Similarly, skewed ternary catalysts of alumina-zirconia are also prepared which are coded AMZ-39-0-49 and AMZ-29-0-59. In these catalysts, the alumina in balanced alumina-zirconia catalysts is partially replaced with zirconia. Only balanced catalyst composition is prepared for the magnesia-zirconia ternary composition (AMZ-0-44-44). Skewed catalysts of this composition are not included in the study.

The quaternary catalysts comprise catalysts containing all three major components alumina, magnesia, and zirconia, where two of the components have similar concentration and remaining component has a higher concentration. These supports are coded AMZ-44-22-22 (alumina-magnesia-zirconia) or AMZ-22-44-22 or AMZ-22-22-44. These too contain nominal 5.4wt% each of lanthana and ceria.

Since published literature reports that impregnation of promoter components has an adverse effect on activity [17,22], such as masking the surface of the active phase, co-precipitation is selected as the method of incorporating the promoters.

The nitrate salt precursors of aluminium, magnesium, zirconium, lanthanum, and cerium are dissolved in a predetermined quantity of demineralized water to prepare

aqueous solutions. Depending on the support composition a combination of these solutions is prepared to achieve the target composition of the support. This solution is agitated at 300 RPM and heated to 70±5°C using a hot plate. Strike precipitation is carried out by adding a solution of 0.5 M NaOH to the solution of metal nitrates till the pH reaches 8.0 ±0.2 units. The temperature is maintained at 70±5°C throughout the precipitation step. The precipitates are aged at 70±5°C for 1 hour in the mother liquor followed by filtration. The filtrate is analyzed for the presence of residual elements. The concentrations of all the elements were less than 200 ppm indicating efficient precipitation. The precipitate is thoroughly washed with demineralized water having a temperature of 75-80°C till Na_2O content decreases to ≤ 500 ppm in the precipitates. The precipitate is dried at 120°C for 12 hours in an oven. Samples of all the composites at the as-synthesized dried stage were retained for DSC-TG and FTIR studies. The remaining dried precipitates were calcined in air at 650°C, for 4 hours in an electrically heated Nabertherm LH40 furnace. The ramping up to 650°C was done by attaining 250°C in 2 hours, 450°C in 2 hours and 550°C in 2 hours. The actual composition of the composites as determined by ICP-OES analysis is presented in Table 1.

The ternary composition design diagram of the supports is shown in Figure 1. Rare Earths Lanthana and Ceria are excluded from Figure 1.

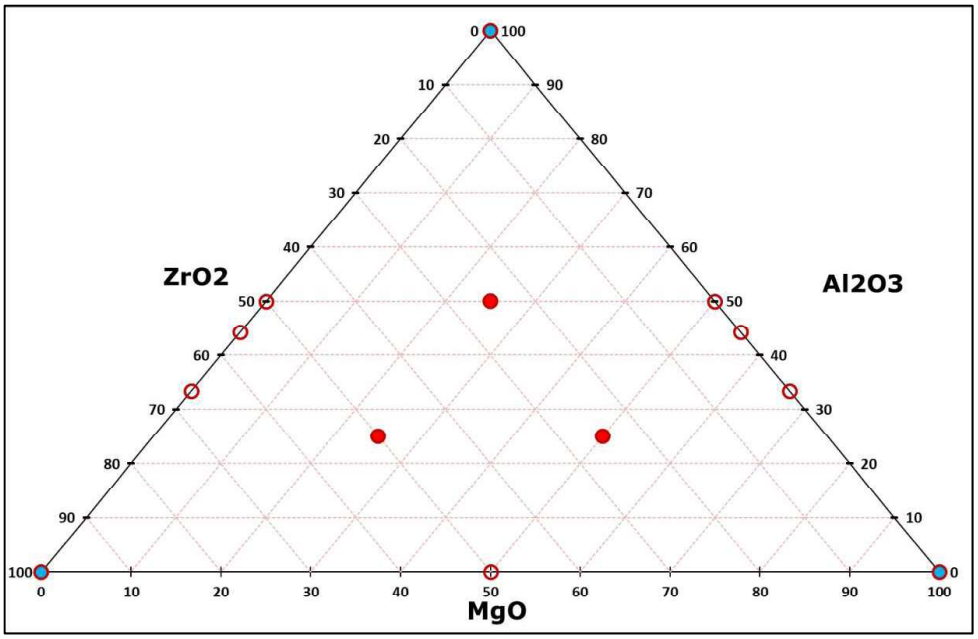

Figure 1: Design composition space of the composites (wt%), excluding rare earth components La and Ce; Binary composites (filled blue circles), Ternary composites (open red circles), Quaternary composites (filled red circles).

Table 1: Chemical composition of calcined composites.

Support	La_2O_3 (wt%)	CeO_2 (wt%)	Al_2O_3 (wt%)	MgO (wt%)	ZrO_2 (wt%)
AMZ-89-0-0	5.38 (0.12)	5.38 (0.12)	89.24 (0.34)	0.00	0.00
AMZ-0-89-0	5.41 (0.14)	5.39 (0.13)	0.00	89.2 (0.37)	0.00
AMZ-0-0-89	5.44 (0.12)	5.41 (0.15)	0.00	0.00	89.15 (0.36)
AMZ-44-44-0	5.35 (0.15)	5.38 (0.16)	44.60 (0.26)	44.67 (0.24)	0.00
AMZ-0-44-44	5.31 (0.12)	5.37 (0.12)	0.00	45.61 (0.24)	43.71 (0.26)
AMZ-44-0-44	5.39 (0.15)	5.43 (0.12)	44.51 (0.25)	0.00	44.67 (0.27)
AMZ-39-49-0	5.44 (0.13)	5.45 (0.13)	39.41 (0.31)	49.70 (0.29)	0.00
AMZ-29-59-0	5.41 (0.15)	5.48 (0.14)	29.65 (0.27)	59.46 (0.32)	0.00
AMZ-39-0-49	5.36 (0.12)	5.49 (0.14)	39.32 (0.30)	0.00	49.83 (0.3)
AMZ-29-0-59	5.61 (0.11)	5.43 (0.14)	29.65 (0.23)	0.00	59.31 (0.29)
AMZ-44-22-22	5.45 (0.13)	5.39 (0.12)	44.41 (0.27)	22.31 (0.19)	22.44 (0.18)
AMZ-22-44-22	5.40 (0.14)	5.40 (0.13)	22.19 (0.19)	44.31 (0.24)	22.70 (0.20)
AMZ-22-22-44	5.44 (0.13)	5.43 (0.12)	22.31 (0.18)	22.29 (0.19)	44.53 (0.25)

Note: Values of Standard Deviation for analysis of chemical composition are given in parentheses.

The generic formula of the composites on a weight fraction basis is:

$$0.0541\ La_2O_3\ 0.0541\ CeO_2\ 0.892[(Al_2O_3)_x\ (MgO)_y\ (ZrO_2)_z]$$

where x, y, z range from 0-0.892

Since hydrothermal stability is an important property for catalysts used in steam reforming, a part of all the calcined support samples were subjected to hydrothermal aging. This comprised heating the samples at 750°C for 4 hours in a furnace in the presence of steam. Water was fed to the furnace at a flow rate of 0.04 ml/min with a Watson-Marlow peristaltic pump. The properties of the hydrothermally aged samples were compared with the properties of samples that were calcined in the absence of water to assess their hydrothermal stability.

2.2.3: Material Characterization

Determination of the composition of the catalysts: The calcined samples of the supports are digested and dissolved in an acidic solution having a mixture of Hydrofluoric acid and Nitric Acid at 120-150°C. An ICP-OES analyzer (Thermoscientific iCAP 6000 series) is used for determining the concentration of La, Ce, Al, Mg and Zr in the supports. The sodium oxide (Na_2O) content of the supports is determined using a Microprocessor Based Flame Photometer of Model: µFlameCal5, ANALAB make.

Determination of XRD phase and crystallite size: Phase purity of the supports is determined with a Bruker D8 FOCUS X-ray diffractometer with a Cu Kα source, wavelength 1.5406 Å. Samples are scanned in the 2-θ range of 5° to 80° at 0.04° per min rate and 0.25 step/s. The phase is identified by matching with a pattern from the in-built XRD library PDF-4. The crystallite sizes of different phases are determined from the most intense XRD peak using the Scherrer equation.

$$D=K\lambda/(\beta \cos \theta)$$

where D is the mean size of crystallites (nm), K is the crystallite shape factor, λ is the X-ray wavelength, B is the full width at half the maximum (FWHM) in radians of the X-ray diffraction peak and θ is the Braggs' angle (degrees.)

Determination of Microstructure: A Quantachrome QUADRASORB SI IV N_2 physisorption unit is used for measuring specific surface area, pore volume, pore size distribution and type of isotherm. The specific surface area is calculated using the BET (Brunauer-Emmet-Teller) equation. Pore volume is determined at P/P_0 0.99. Pore size distribution is determined from the desorption leg of the isotherm using the BJH method. Samples were degassed under vacuum at 300°C using a FloVac instrument for 3 hours before measurement.

Thermogravimetric analysis (DSC-TG): It is performed from ambient temp to 900°C with a temperature ramp rate of 10°C per minute in air. The flow rate of air is 100 ml/min. A TA make instrument model Q600 DSC-TG is used for this measurement.

The acidity of Support using Ammonia TPD (NH_3-TPD) Technique: The acidity of the supports is measured by the ammonia TPD technique. A Micromeritics Autochem-2920 instrument is used for this purpose. Samples are first heated in air to 500°C to remove adsorbed substances. They are then cooled to 50°C and saturated with a flow of NH_3 in Helium at 50°C. A calibration gas mixture with composition 5 vol% NH_3 in Helium is used for quantification. The flow rate of this gas is 50 ml/min for a duration of 30 minutes. The samples are then flushed for 1 hour with a flow of 10 ml/min Helium to desorb weakly adsorbed NH_3. The TPD is recorded by ramping the temperature from 50°C to 900°C at 10°C/min in a flow of He.

Oxygen storage capacity (OSC): It is measured using O_2/CO titrations in the Autochem-2920 instrument using the method of Madier et.al. [32]. This comprises reducing the supports and then oxidizing them by pulsing oxygen till saturation. After oxidation, carbon monoxide is pulsed to determine the oxygen storage capacity based on the amount of carbon dioxide formed.

Fourier Transform Infra-red spectroscopy (FTIR): FTIR is performed with a Perkin Elmer Spectrum GX instrument over the wavenumber range 400 to 4000 cm^{-1}. A scan rate of 0.2 cm^{-1}/s is maintained. The samples are pelletized using KBr.

Acid-Base Character of Supports: In addition to NH_3-TPD, the acid-base character of the supports is studied through the decomposition of 2-methyl-3-butyn-2-ol (MBOH) [36] in a flow-through glass reactor. This reaction was developed by researchers from Rhone Poulenc. 0.55 grams of sample sized to 0.55-0.85 mm fraction is used for the study. The reaction is carried out for a duration of 8 hours on stream at 220°C, ambient pressure and 0.8 h^{-1} space velocity (GHSV). The sample is first pre-activated at 300°C for 2 hours in pure dry nitrogen. The temperature is then decreased to 220°C and MBOH is fed by bubbling nitrogen at 50 ml/min through a bubbler which is maintained at 30°C by flowing thermostated water in its jacket. The product is analyzed online with an Agilent 7890B Gas Chromatograph using INNOWAX capillary column (0.53 mm ID, 30m length, 0.5μm film thickness) and an FID detector. Response factor corrected area normalization is used for the quantification of the product stream.

% Conversion of MBOH is calculated as below:

$$\text{Conversion } \% = \frac{\text{Concentration of MBOH in reactant} - \text{MBOH concentration in product}}{\text{Concentration of MBOH in reactant}} \times 100$$

Product selectivity is calculated as below:

$$S_i = \frac{\text{Mol component i produced}}{\text{Mol MBOH converted}}$$

The decay constant for deactivation is determined using an empirical Power law equation.

$$A = c * t^{kd}$$

Where A = activity at time t which is the ratio of conversion at time t / initial conversion, t = time on stream (min), kd = decay constant and c = scaling factor which is constant.

2.3: Results and Discussion

2.3.1:Chemical Composition of Supports

The composition of the calcined samples as determined by ICP-OES is shown in Table 1 above. The nomenclature used is AMZ-#-@-$, where #, @ and $ represent wt% of alumina, magnesia, and zirconia respectively. La_2O_3 and CeO_2 content is ~5.4wt% each in all the samples and is therefore excluded from the nomenclature. Na_2O content as determined by Flame Photometry is < 500 ppm in all the samples.

2.3.2: Microstructure of the Supports

The trend of BET-specific surface area of the calcined and hydrothermally aged composites is compared in Figure 2 below.

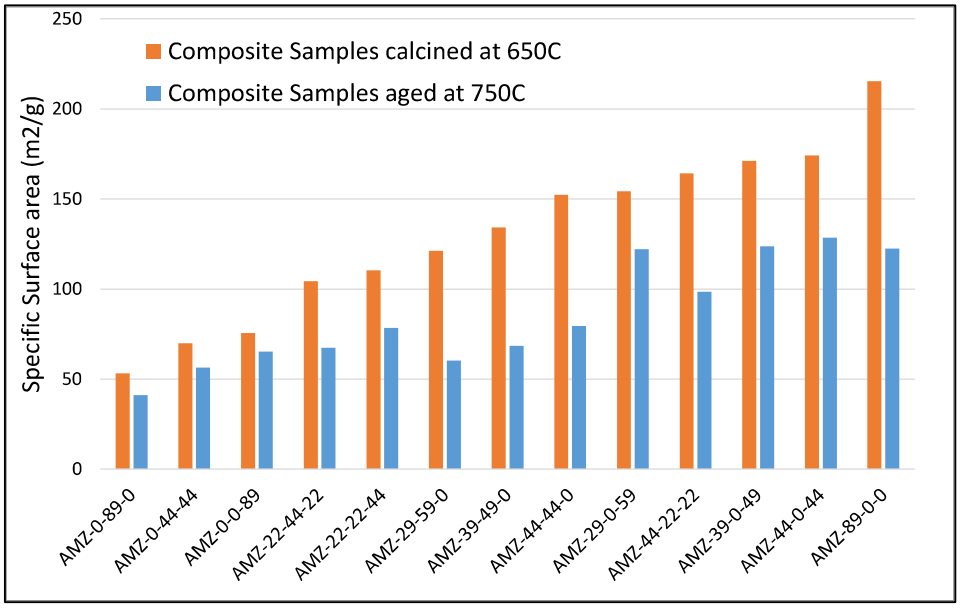

Figure 2: BET-specific surface area of composites calcined at 650°C and hydrothermally aged at 750°C.

As seen from Figure 2, the binary Al_2O_3 support (AMZ-89-0-0) which does not contain zirconia and magnesia shows the highest specific surface area (215 m^2/g) amongst the binary supports and also across all the samples. This is followed by the binary zirconia sample AMZ-0-0-89 (76 m^2/g) and the magnesia sample AMZ-0-89-0 (53 m^2/g). There is a significant difference in the specific surface area of binary alumina and the remaining two binary samples.

Amongst the ternary supports, specific surface area decreases in the order AMZ-44-0-44>AMZ-39-0-49>AMZ-29-0-59>AMZ44-44-0>AMZ-39-49-0>AMZ-29-59-0>AMZ-0-44-44. Thus, the ternary support of Al-Zr with balanced composition shows the highest surface area followed by the supports with skewed Al-Zr composition. All the ternary Al-Zr supports show higher specific surface area than the ternary Al-Mg supports. Within the ternary Al-Mg supports the trend is similar to that of the ternary Al-Zr supports. The support with balanced Al-Mg composition shows higher surface area than the supports with skewed Al-Mg composition. It is clear that in both the Al-Zr and Al-Mg series surface area decreases with increasing concentration of Zr or Mg. The trend of change in the specific surface area of ternary Al-Mg and Al-Zr supports is compared with the arithmetic mean of the surface areas of the corresponding binary supports in Figure 3 below.

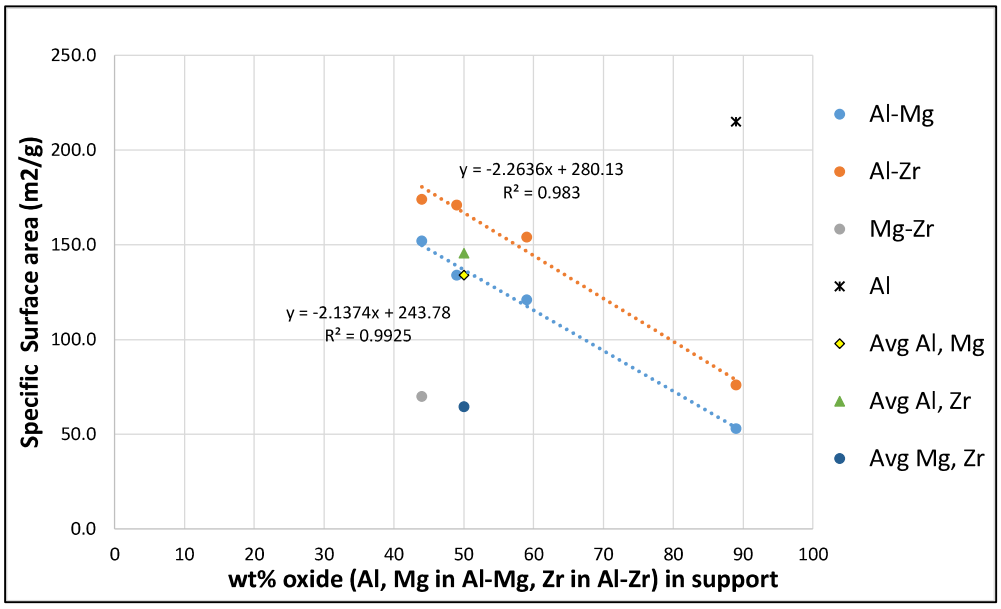

Figure 3: The trend of change in the specific surface area of ternary Al-Mg and Al-Zr supports relative to arithmetic mean of the binaries.

The points on the right-hand side of the plot (with composition 89wt%) show binary supports. Decreasing values on X axis represent progressive substitution of Mg (in ternary Al-Mg) or Zr (in ternary Al-Zr) with Al. As seen from Figure 3 there is an almost linear increase in surface area when magnesia or zirconia are substituted with alumina. Further, the ternary Al-Zr supports show about 30 m^2/g higher surface area than corresponding Al-Mg supports. Still, further, the value of the arithmetic mean of the binary Al and Mg supports falls exactly on the trend line of ternary Al-Mg supports. Whereas the arithmetic mean of binary Al and Zr supports falls 25 units below the trend line of Al-Zr ternary supports. P-XRD indicates the formation of Magnesium aluminate spinel and zirconia-alumina solid solution. Thus, the formation of magnesium aluminate spinel does not change surface area relative to the arithmetic mean of the individual binary components, whereas zirconia alumina solid solution increases the surface area by about 25 m^2/g. The latter could be due to the formation of solid solutions as indicated by P-XRD. The composite of magnesia and zirconia (AMZ-0-44-44) shows the lowest specific surface area (70 m^2/g). Its value is close to that of the arithmetic mean of binary Mg and Zr support.

Amongst the quaternary supports, the trend is AMZ-44-22-22 > AMZ-22-22-44 > AMZ-22-44-22. This trend is similar to that of the binary supports. The AMZ-44-22-22 (alumina-rich) support shows a significantly higher surface area than the remaining two quaternary supports. This support shows the surface area between the skewed Al-

Zr supports, whereas the AMZ-22-22-44 support (zirconia rich) shows a surface area that is lower than that of all the ternary Al-Mg supports.

The regression plot of BET specific surface area versus Al content of the supports is shown in Figure 4 below. As seen from this Figure the specific surface area shows a reasonable linear correlation with the Al_2O_3 content of the composites (Equation 1 below).

Sp. Surface area = 1.8303 * wt% of alumina + 73.68 with $R^2 = 0.889$ (Equation 1)

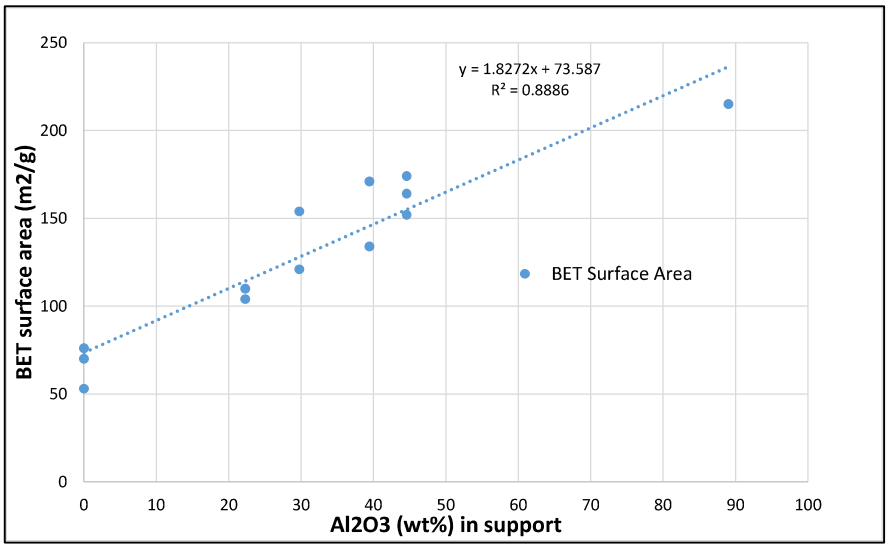

Figure 4: Relation between BET-specific surface area and alumina content of the support.

As seen from Figure 4 there is a reasonable correlation between the alumina content of the supports and the specific surface area of the supports. The correlation constant is 0.889. Further, the Y-intercept approximates the measured specific surface areas of composites which are free from alumina viz. binary support of neat magnesia (53 m^2/g) or zirconia (76 m^2/g) or ternary support of magnesia with zirconia (70 m^2/g). Outliers to the trend are mostly ternary supports of alumina and zirconia and binary supports containing either magnesia or alumina. As seen in Figure 3 the specific surface area of ternary alumina-zirconia is higher than the arithmetic mean of the individual binary alumina and zirconia support. Hence the reason for the poor fit of these supports appears to be due to the formation of a solid solution between zirconia and alumina. XRD plots in Appendix 3 (Figure A3.1, A3.3, A3.6, A3.9, A3.10) confirm this.

Thus, Al_2O_3 is the main contributor to the specific surface area of these supports. Chengxi et.al. [9] have reported a specific surface area of 47 m^2/g and pore volume of 0.11 ml/g for ZrO_2 prepared by gelation and further calcined at 500°C. These values

compare well with the surface area and pore volume of the corresponding sample of the current study, AMZ-0-0-89, (~76 m2/g and 0.31 ml/g respectively).

The effect of support composition on the hydrothermal stability of the supports is expressed as a percentage decrease in the specific surface area of the supports pre-calcined at 650°C upon further hydrothermal treatment at 750°C, 4 hours with water feed (0.04 ml/min). This is shown in Figure 5 below.

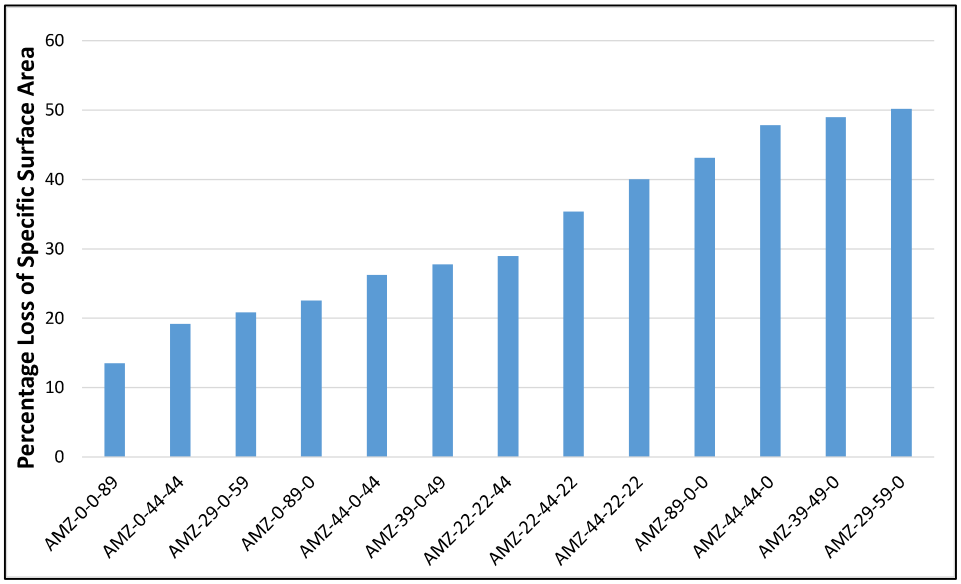

Figure 5: Percentage Loss of specific surface area for various supports after Hydrothermal treatment

As seen from Figure 5 above, all the supports lose surface area upon hydrothermal aging. Amongst the binary supports the alumina support (AMZ-89-0-0) shows a significantly higher decrease than zirconia (AMZ-0-0-89) or magnesia (AMZ-0-89-0) binary supports upon hydrothermal ageing. The trend in decrease is alumina > zirconia > magnesia.

Amongst the ternary supports the skewed alumina-magnesia supports show a higher percentage loss of surface area than the balanced alumina-magnesia supports. Between these supports percentage loss in surface area increases with increasing magnesia in the support. The alumina-zirconia ternary supports show a significantly smaller percentage decrease in surface area than the alumina-magnesia supports. The percentage loss of surface area decreases with increasing zirconia content. Amongst the quaternary supports the alumina-rich support AMZ-44-22-22 shows a significantly higher percentage loss of surface area than the magnesia-rich support. The zirconia-rich support shows the smallest percentage decrease in surface area. Across the series, the

trend of decrease is skewed ternary Al_2O_3-MgO > binary Al_2O_3 > Al_2O_3-rich quaternary >Magnesia-rich quaternary >zirconia-rich quaternary > skewed ternary Al_2O_3-ZrO2> balanced Al_2O_3-ZrO_2 > binary magnesia > skewed ternary Al_2O_3-ZrO_2 > ternary MgO-ZrO_2>binary zirconia. Thus, although binary magnesia shows a lower loss of surface area than most of the supports, its combination with alumina results in an overall increase in loss of surface area in ternary Al_2O_3-MgO supports relative to binary alumina. In contrast, binary zirconia, which shows the smallest decrease in surface area over the entire series lends hydrothermal stability to alumina in ternary Al_2O_3-ZrO_2 and also all the quaternary supports. Thus, zirconia lends hydrothermal stability and helps to retain specific surface area whereas magnesia does not. Zirconia also lends hydrothermal stability to the ternary MgO-ZrO_2 support which shows a smaller percentage decrease than binary magnesia.

The specific surface area of AMZ-89-0-0 decreases by 43% whereas that of pure γ-Al_2O_3 (without rare earths) decreases by 75%. Thus, even low molar ratios (0.019 and 0.036) of La_2O_3 and CeO_2 impart hydrothermal stability to alumina. Increasing the amount of lanthana or ceria decreases specific surface area [31], which is not desirable. The results in Figure 2 show that, although the specific surface area of zirconia composite (AMZ-0-0-89) is low (65 m^2/g) when alumina is partially substituted with zirconia (in supports AMZ-44-0-44, AMZ-39-0-49 and AMZ-29-0-59), the latter show retention of specific surface area (122-129 m^2/g) which is at the same level as the alumina composite (AMZ-89-0-0) after aging. The formation of a solid solution (as observed in P-XRD) is attributed to the above observation. Zirconia also improves OSC as shown in a later section. Thus, zirconia shows synergistic behaviour with alumina and ceria.

The effect of support composition on the pore volume of composites calcined at 650°C is shown in Figure 6 below:

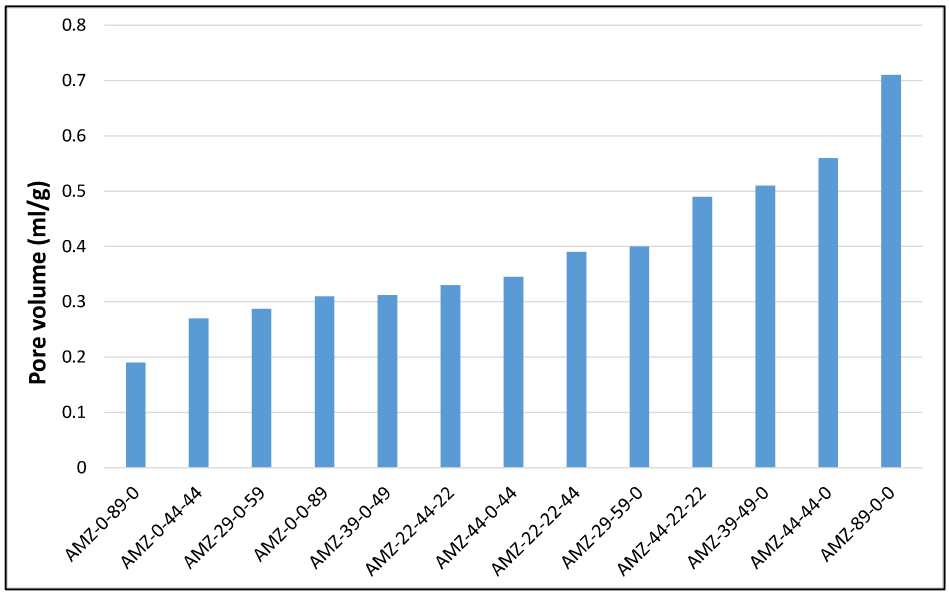

Figure 6: Pore volume of composites calcined at 650°C.

As seen from Figure 6 above, amongst the binary supports the alumina support (89-0-0) shows significantly higher pore volume than the zirconia support followed by the magnesia support. The binary alumina shows the highest pore volume across all the series of supports.

The trend for ternary catalysts is Balanced Al_2O_3-MgO>skewed Al_2O_3-MgO> balanced Al_2O_3-ZrO_2 > skewed Al_2O_3-ZrO_2 > MgO-ZrO_2. Thus, pore volume decreases when MgO or ZrO_2 are combined with Al_2O_3. MgO shows a smaller decrease in pore volume than ZrO_2. The ternary MgO-ZrO_2 shows the smallest pore volume not only within ternary catalysts but across the entire series of catalysts. Pore volume decreases with a progressive increase in the ZrO_2 content of the support. Seung Han et.al. [41] have studied 10%Ni-Al_2O_3-ZrO_2 xerogel catalysts with different Zr/Al mole ratios (0-0.4), which are prepared by single-step epoxide is driven sol-gel method. They too report a similar trend for pore volume.

Amongst the quaternary catalysts, the trend is Al_2O_3-rich > ZrO_2-rich > MgO-rich.

The trend across all the series is Binary Al_2O_3>Balanced Al_2O_3-MgO>skewed Al_2O_3-MgO>Al_2O_3 rich quaternary > skewed Al_2O_3-MgO > ZrO_2-rich quaternary > balanced Al_2O_3-ZrO_2 > MgO rich quaternary > skewed Al_2O_3-ZrO_2 > Binary ZrO_2 > skewed Al_2O_3-ZrO_2 29-0-59> ternary MgO-ZrO_2 > binary Magnesia.

Although binary magnesia support shows smaller pore volume than binary zirconia support, when combined with alumina the former shows higher pore volume than the latter for ternary supports whereas, the trend reverses for quaternary supports. The formation of Magnesium aluminate spinel and zirconia-alumina solid solution appears to contribute to these trends. (Refer to Appendix 3 for XRD data)

The effect of composition on the percentage change in pore volume after hydrothermal aging of the supports at 750°C for 4 hours is shown in Figure 7 below:

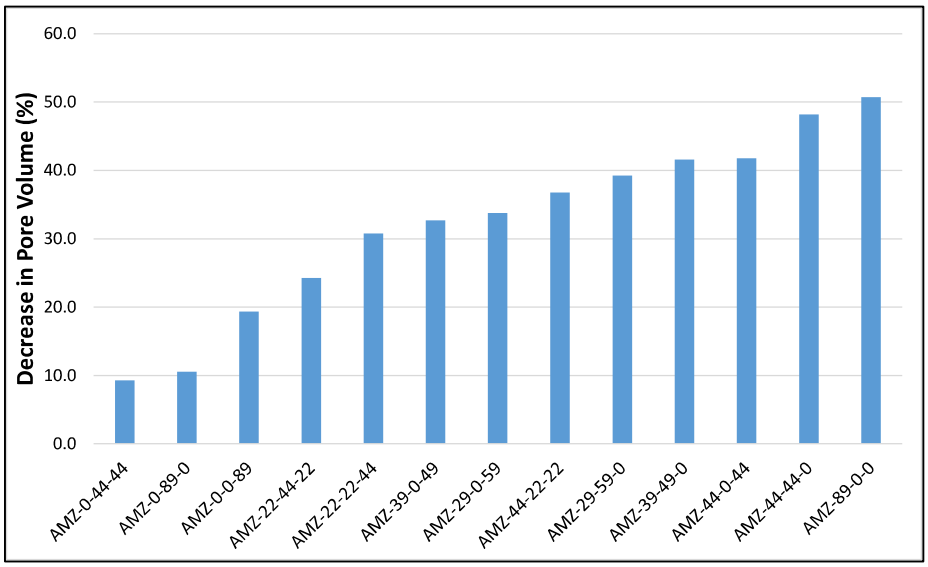

Figure 7: Percentage decrease in pore volume after hydrothermal aging of the supports

As seen from Figure 7 all the supports show a decrease in pore volume upon hydrothermal aging. Amongst the binary catalysts, the trend of the percentage decrease in pore volume is AMZ-89-0-0>AMZ-0-0-89>AMZ-0-89-0. Thus, binary alumina loses the highest pore volume and binary magnesia the least. Amongst the ternary supports both the balanced Al_2O_3-MgO and Al_2O_3-ZrO_2 lose the highest percentage pore volume followed by the skewed Al_2O_3-MgO and lastly the skewed Al_2O_3-ZrO_2. The trend for quaternary catalysts is Al_2O_3-rich > Zirconia-rich > Magnesia-rich. Across the series, the trend is binary Al_2O_3>Balanced Al_2O_3-MgO>Balanced Al_2O_3-ZrO_2>skewed Al_2O_3-MgO>Al-rich quaternary>skewed Al_2O_3-ZrO_2>ZrO_2-rich quaternary>MgO-rich quaternary>binary ZrO_2>binary MgO>ternary MgO-ZrO_2. Thus, both magnesia and zirconia lend hydrothermal support to Al_2O_3 for retaining pore volume. Between the two zirconia is more effective in the case of ternary supports whereas magnesia is more effective for quaternary supports.

The effect of support composition on the median pore size of the supports is shown in Figure 8 below. As seen from this Figure all the supports are mesoporous with average pore diameter ranging from 79 Å to 122 Å.

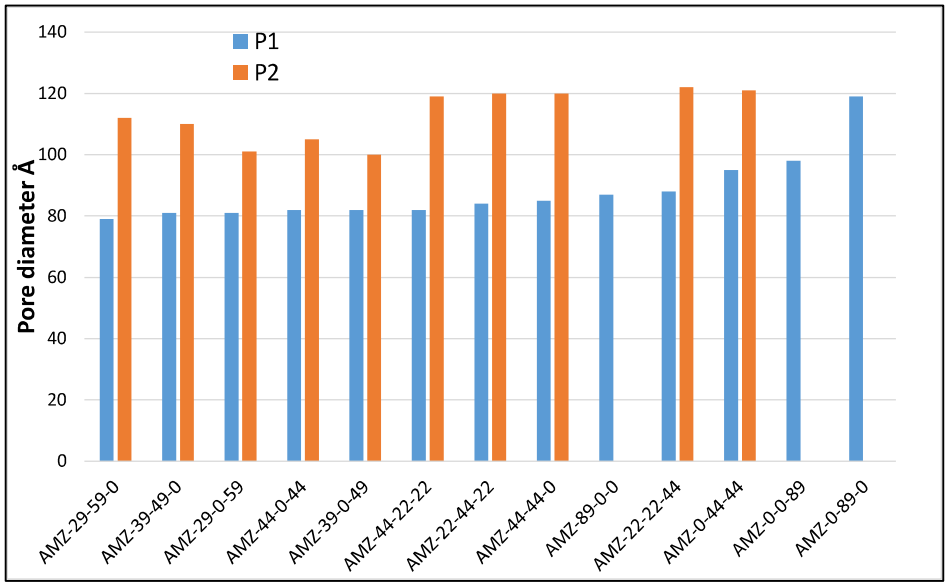

Figure 8: Median pore diameter of composites calcined at 650°C.

Further, all the binary supports present unimodal pore size distribution with median pore diameter ranging from 87Å -119Å. In contrast, the ternary and quaternary supports present bimodal distribution with one set of pores ranging from 79 to 95Å and a second set ranging from 100Å - 122Å.

The average pore diameter decreases in the order $MgO>ZrO_2>Al_2O_3$ for the binary supports. The trend of the pores in the range 79Å -119Å for ternary supports is ternary $MgO\text{-}ZrO_2$>Balanced $Al_2O_3\text{-}MgO$>skewed $Al_2O_3\text{-}ZrO_2$>Balanced $Al_2O_3\text{-}ZrO_2$>skewed $Al_2O_3\text{-}ZrO_2$ >skewed $Al_2O_3\text{-}MgO$. The corresponding trend for quaternary supports is ZrO_2-rich>MgO-rich>Al_2O_3-rich. Thus, Al_2O_3 decreases the pore diameter of MgO significantly more than ZrO_2 in both ternary and quaternary supports. Further, there is no significant difference in pore size between balanced and skewed $Al_2O_3\text{-}ZrO_2$ ternary supports whereas the balanced $Al_2O_3\text{-}MgO$ support shows a higher pore diameter than its skewed counterparts.

The trend of the set of larger pores with diameter 100Å -122Å is Quaternary ZrO_2-rich>Ternary $MgO\text{-}ZrO_2$> balanced $Al_2O_3\text{-}MgO$ = Quaternary MgO-rich > Quaternary Al_2O_3-rich> skewed $Al_2O_3\text{-}MgO$>balanced $Al_2O_3\text{-}ZrO_2$>skewed $Al_2O_3\text{-}ZrO_2$.

The trend for larger pores in ternary supports is different from that for the smaller pores (79Å -119Å). The Al_2O_3-MgO ternary supports have larger pores than ternary Al_2O_3-ZrO_2. Quaternary ZrO_2-rich support shows higher pore size than ternary AMZ-0-44-44. The former shows the largest pore diameter across the entire set of supports. The ternary composites which contain magnesia along with zirconia (AMZ-0-44-44) or alumina (AMZ-44-44-0) and all three quaternary supports show the highest pore diameters in the narrow range 119Å -122 Å.

The change in median pore diameter (MPDA) of the supports upon hydrothermal aging is shown in Figure 9 below:

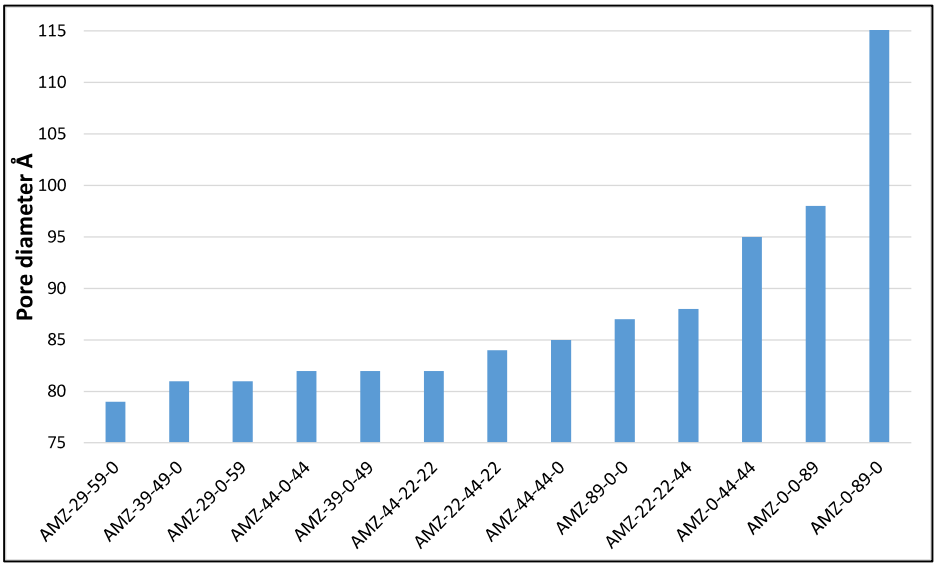

Figure 9: Median pore diameter (MPDA) of the supports upon hydrothermal aging

Comparing the values in Figure 8 with those in Figure 9, it is observed that hydrothermal aging did not affect pore diameter significantly.

The effect of the composition of the support on pore diameter distribution is shown in Figure 10. The pore diameter is divided into three ranges <60Å, 60-150 Å and >150 Å.

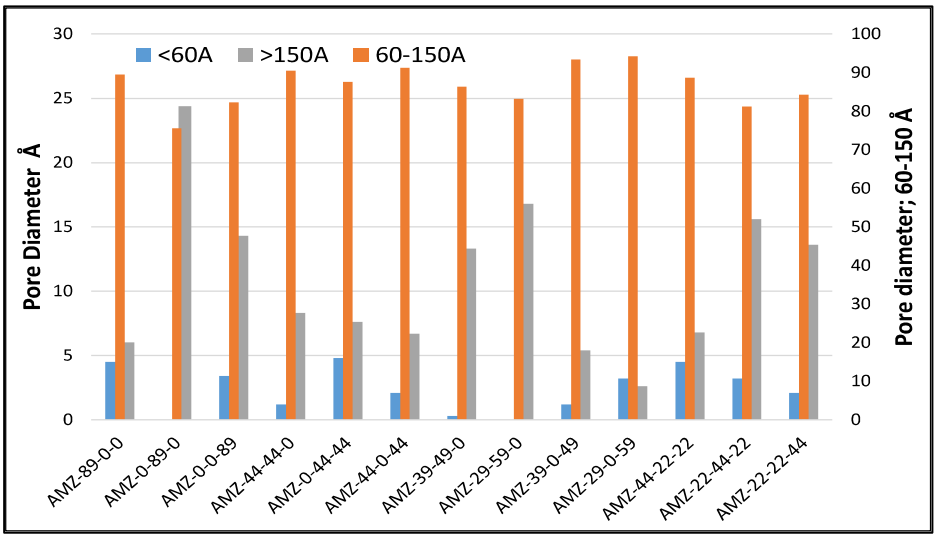

Figure 10: Pore Diameter Distribution of composites calcined at 650°C

As seen from the above Figure 10 the supports are largely mesoporous in nature with a mesopore fraction above 99.6% for all the samples. It remains same even as per IUPAC nomenclature micropores <2 nm, mesopores 2-50 nm and macropores >50 nm

Interestingly all thirteen supports show two distinct types of isotherms depending on whether they contain alumina or not. Representative isotherms of these two types are shown in Figures 11 (i, ii). The isotherms of all supports are presented in Appendix 1

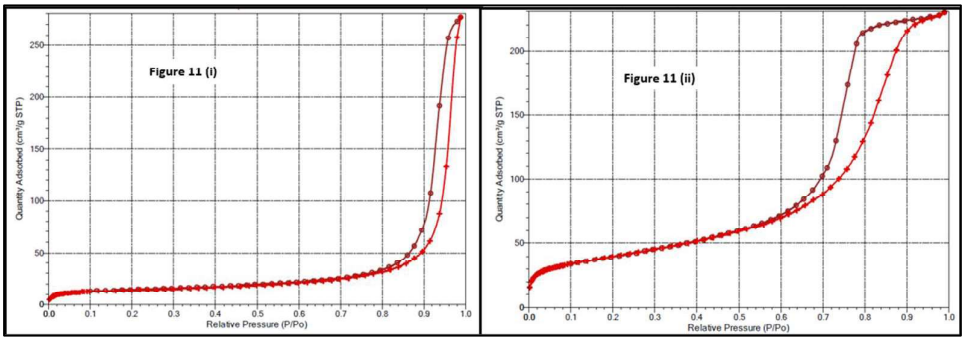

Figure 11: Isotherms representative of composites i) not containing alumina. ii) containing alumina

The isotherms in Figures 11, (i) and (ii) are of type IVa isotherms with a clear hysteresis loop which indicates mesoporosity. Within these, the supports which contain alumina show an adsorption branch of type H2(a) and a desorption branch of H2(b) (Figure 11 (ii)). This is reported to indicate pore blocking. Supports that do not contain alumina present isotherms with type H3 hysteresis loop (Figure 11 (i)) which indicates the morphology of non-rigid aggregates of the plate-like particles or a network of macropores that are incompletely filled with pore condensate [39]. This also reflects in

values of pore volume (Figure 6) wherein supports that do not contain alumina (AMZ-0-89-0) and (AMZ-0-44-44) show the lowest pore volume.

2.3.3: Acidity by NH_3-TPD

Acidity and acid strength were estimated from the results of ammonia temperature programmed desorption studies. The method is described in the methods section above. The plots of desorption of NH_3 with temperature for the supports are presented in Appendix 2. The maximum in temperature (Tmax) of TPD peaks is shown in Figure 12 below. As seen from this Figure all the samples show two desorption peaks of ammonia. The maxima (Tmax) of the peak at a lower temperature is designated 'T1' and the maxima of the peak at a higher temperature is designated 'T2' in this Figure 12.

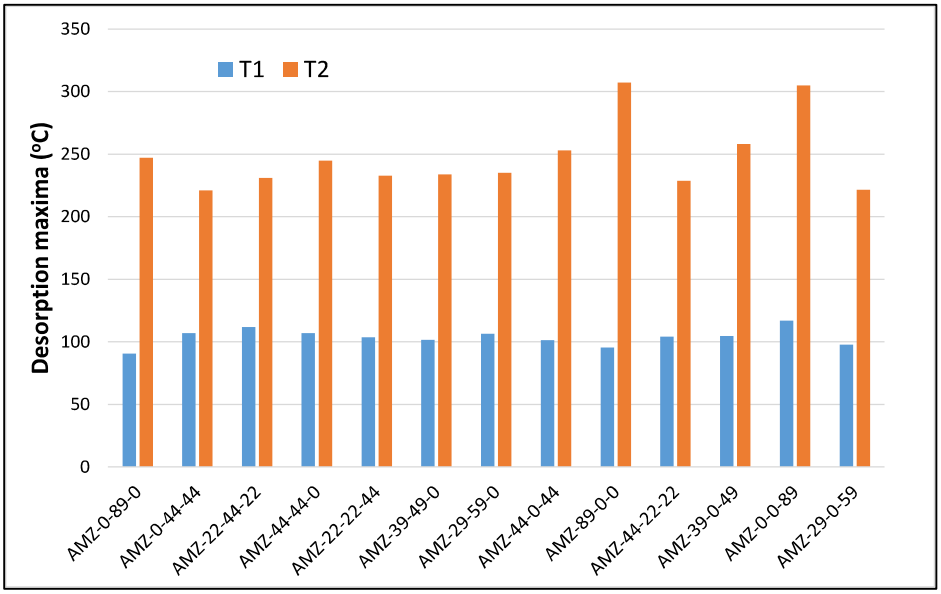

Figure 12: Temperature maxima in NH_3 TPD of composites calcined at 650°C

The maxima of the low-temperature peak which is designated 'T1' range from 90°C to 117 °C across the samples. The low-temperature nature of this peak suggests that ammonia is weakly adsorbed. Between the binary supports, the zirconia-based support (AMZ-0-0-89) shows desorption of ammonia at the highest temperature (117°C) followed by the alumina composite (AMZ-89-0-0) where it desorbs at 95°C. Ammonia desorbs at the lowest temperature, 91°C, in the case of the magnesia composite (AMZ-0-89-0). The remaining samples, viz. ternary Al-Mg and Al-Zr and the quaternary supports show desorption of ammonia at an intermediate value of temperature ranging from 101°C -112°C. Within the respective ternary supports, there is no clear trend between balanced and skewed compositions or between Al_2O_3-MgO

and Al_2O_3-ZrO_2 compositions. The difference in acid strength of this peak between the quaternary supports is also marginal.

The second peak 'T2' manifests at a significantly higher temperature, in the range of 221°C -307°C indicating strong adsorption/chemisorption of ammonia and hence represents strong acidity. The trend of this peak with support composition is as follows. Binary supports which contain only alumina (AMZ-89-0-0) or zirconia (AMZ-0-0-89) show peak maxima at 307°C and 305°C respectively, which is significantly higher than the remaining supports. This is an indication of higher acid strength. The binary magnesia support (AMZ-0-89-0) shows significantly lower acid strength (247°C) which is understandable because it is an oxide of alkaline earth metal. However, although the binary alumina and zirconia supports show desorption of the second peak at significantly higher temperatures than the remaining samples, their ternary supports (AMZ-44-0-44, AMZ-39-0-49 and AMZ-29-0-59) show peak maxima which are at a significantly lower temperature (221°C -258°C) indicating a decrease in acid strength. The reason for the decrease in acid strength is attributed to the formation of a solid solution between the two oxides. Results of P-XRD show that the crystalline pattern of t-ZrO2 becomes diffused and peaks of γ-Al2O3 are absent (Appendix 3 Figures A3.6, A3.9, A3.10) indicating the formation of a solid solution. Results of DSC-TG also show a significant difference in trends thus supporting this observation (refer Figure 16 below). This is discussed in the sections below.

The sample of binary magnesia (AMZ-0-89-0) shows Tmax at 247°C. Whereas its ternary supports with Al_2O_3 show maxima in the range of 230°C -246°C, which is not very different from that of binary MgO. The balanced Al_2O_3-MgO shows slightly higher acid strength than the skewed compositions. Thus, the decrease in acid strength relative to binary MgO is much smaller than in the case of ternary Al_2O_3-ZrO_2, relative to binary ZrO_2.

Between the three ternary compositions, the trend of the acid strength of supports with balanced composition is Al_2O_3-ZrO_2>Al_2O_3-MgO>MgO-ZrO_2. Thus, magnesia decreases the acid strength of zirconia to a higher extent than alumina.

The quaternary supports show the trend Mg-rich = Zr-rich >Al-rich. This is different from that of the binary or ternary compositions, possibly due to formation of solid solutions.

Total acidity and the ratio of strong acidity to weak acidity of the supports is shown in Figure 13 below.

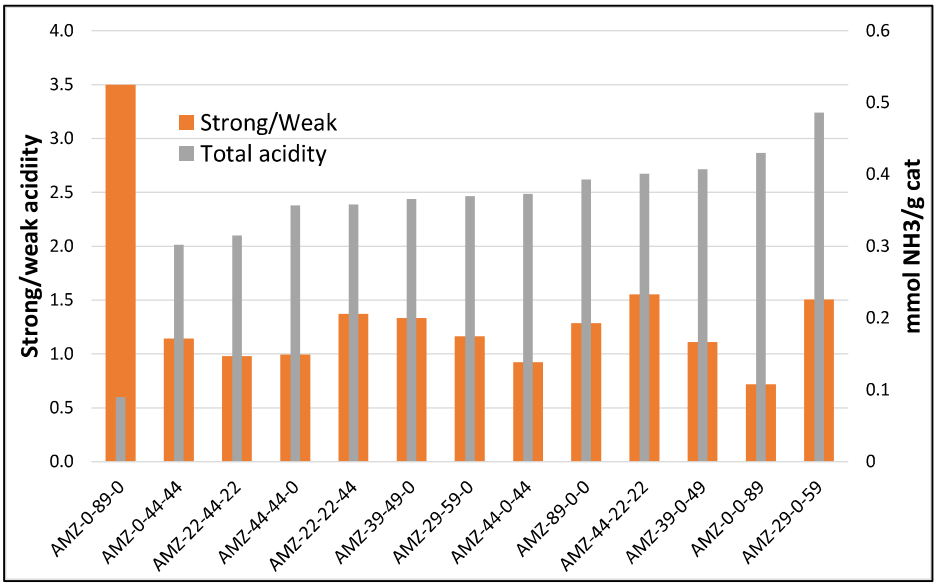

Figure 13: Total acidity and the ratio of strong: weak acidity by NH_3 TPD

The trend of total acidity of binary supports is Zirconia > Alumina >> Magnesia. The ratio of strong to weak acidity follows the trend Magnesia >>alumina>zirconia, which is opposite that of total acidity. It is interesting to note that binary zirconia, which shows high total acidity, shows a significantly low ratio amongst all the supports whereas magnesia, which shows lowest total acidity, shows an unusually high ratio.

Amongst the ternary supports the trend of total acidity is Skewed alumina-zirconia > balanced alumina-zirconia > skewed alumina-magnesia > balanced alumina-magnesia > magnesia-zirconia. Thus, magnesia decreases the acidity of zirconia to a larger extent than it decreases the acidity of alumina relative to their binary supports. As regards the ratio of acid strength, this increases with increasing zirconia content of ternary Al_2O_3-ZrO_2 supprots. In the case of the ternary Al_2O_3-MgO supports increasing MgO increases the ratio, but AMZ-29-59-0 shows a smaller ratio than AMZ-39-49-0. The latter shows a ratio close to quaternary AMZ-22-22-44.

The trend of total acidity of quaternary supports is Al_2O_3-rich>ZrO_2-rich>MgO-rich. The ratio of strong to weak acidity shows the same trend.

Across the series the trend for total acidity is skewed Al_2O_3-ZrO_2>binary ZrO_2> skewed Al_2O_3-ZrO_2>Quaternary Al_2O_3-rich>binary Al_2O_3>Balanced Al-Zr>skewed Al-Mg>Quaternary Zr-rich>balanced Al-Mg>Quaternary Mg-rich>ternary Mg-

Zr>binary Mg. Thus, overall supports rich in zirconia or a combination of Al_2O_3 and ZrO_2 show higher acidity whereas supports rich in MgO show lower total acidity. Thus, magnesia and zirconia influence acidity in contrasting ways.

The quaternary supports AMZ-44-22-22 and AMZ-22-22-44 and the ternary composite AMZ-29-0-59 show a significantly higher ratio of strong: weak acidity than the remaining samples. They are relatively rich in either alumina or zirconia. Amongst the quaternary supports, total acidity decreases in the order AMZ-44-22-22 > AMZ-22-22-44 > AMZ-22-44-22. Based on trends of binary supports, AMZ-22-22-44 which is rich in zirconia is expected to have higher acidity than AMZ-44-22-22 which is rich in alumina. This unexpected trend is again attributed to the formation of solid solutions between alumina and zirconia which enhances the acidity significantly. This is analogous to amorphous silica-alumina which is well known to have higher acidity than either silica or alumina. Zirconium has an oxidation state of +4 which is similar to that of Silicon.

Trends of total acidity determined by NH_3 TPD correlate well with those of product selectivity of acetone (formed on basic sites) and Mbyne (formed on acidic sites) in the decomposition of MBOH (shown in sections below). Supports rich in zirconia or alumina show more acid character (present higher selectivity to Mbyne) (Figure 19 (b). whereas supports that are rich in magnesia show higher selectivity to acetone (Figure 18 (b).

2.3.4: X-Ray Diffraction Measurement of Supports

Phase identification of the supports was done using XRD for the powder samples (P-XRD). P-XRD patterns of relevant calcined supports before and after hydro-thermal aging are provided in Appendix 3. Phase identification was done using the JCPDS-International Centre for Diffraction data's powder-XRD library database 'PDF-4+ 2020'. The XRD patterns of the calcined supports before hydrothermal aging indicate the following:

1. Binary Al support AMZ-89-0-0 shows the presence of γ-Al_2O_3 and ceria.
2. Binary Mg support AMZ-0-89-0 shows the presence of magnesia (periclase phase) and ceria.
3. Binary Zr support AMZ-0-0-89 shows the presence of tetragonal zirconia. Either ceria or lanthana is also observed.

4. Ternary Al-Mg supports with balanced composition (AMZ-44-44-0) or skewed composition (AMZ-39-49-0, AMZ-29-59-0) show a clear presence of magnesium aluminate, $MgAl_2O_4$. Traces of γ-Al_2O_3 are seen in the catalyst with a balanced composition. MgO (periclase phase) may be present but masked by peaks of $MgAl_2O_4$.
5. Ternary Al-Zr supports with balanced composition (AMZ-44-0-44) or skewed composition (AMZ-39-0-49, AMZ-29-0-59) show a largely amorphous phase. The peak at about 2Θ 30.2° indicates it is tetragonal zirconia. γ-Al_2O_3 is not present. Zirconia alumina solid solution may be present but masked by peaks of t-zirconia.
6. Quaternary Al-rich support AMZ-44-22-22 shows broad low-intensity peaks of tetragonal zirconia. The broad amorphous nature and near absence of peaks for γ-Al_2O_3 indicate that Zirconia alumina solid solution may also be present. Alumina is barely visible as a small peak at 37.5° and 45.5° 2Θ. Peaks for periclase are absent.
7. The quaternary Mg-rich support AMZ-22-44-22 shows broad low-intensity peaks of tetragonal zirconia. The broad amorphous nature and complete absence of peaks of γ-Al_2O_3 indicate that the alumina exists as a solid solution. Peaks for MgO (periclase) are present.
8. The quaternary Zr rich support AMZ-22-22-44 shows broad low-intensity peaks of tetragonal zirconia. The complete absence of peaks of γ-Al_2O_3 indicates that the alumina exists as a solid solution. Peaks for MgO (periclase) are also absent.

From the above observations it is clear that Al, Mg and Zr react with each other in ternary and quaternary supports to form either magnesium aluminate or a solid solution of zirconia and alumina.

Change in crystallite size upon hydrothermal aging was determined. The 2-θ peaks and their Miller indices (in parenthesis) which were used for calculating a change in crystallite size are listed below: LaO 30.063° (1 1 1), Al_2O_3 45.666° (4 0 0), MgO 42.887° (2 0 0), ZrO_2 30.222° (2 2 0), $MgAl_2O_4$ 42.972° (4 0 0).

The percentage increase in crystallite size after hydrothermal aging of the supports at 750°C for 4 hours is shown in Figure 14 below.

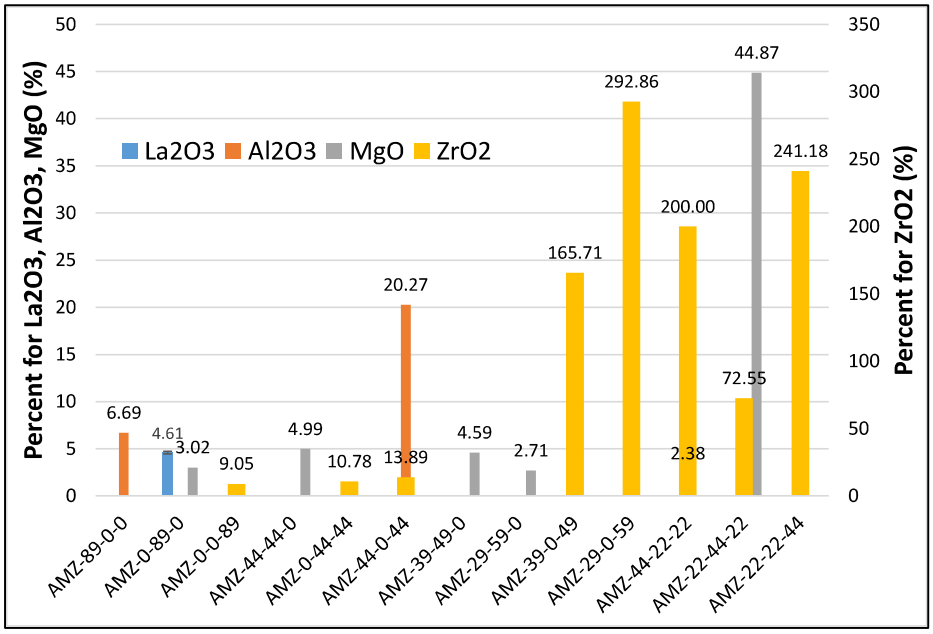

Figure 14: Crystallite growth upon hydrothermal aging of composites at 750°C, 4 hours

As already stated earlier in the chapter, lanthana and ceria are present in a nominal concentration of ~5.4 wt% each in all the supports. The ionic radii of La^{3+} and Ce^{4+} are 1.06 and 1.01 Å respectively. Since these ionic radii are significantly larger than that of Zr^{4+} (0.79Å) these elements cannot dissolve in ZrO_2 (which is the major component). The proximity of XRD lines of these oxides makes it difficult to identify them in multi-component mixtures. Lanthana was detected only in two supports, AMZ-89-0-0 (Appendix 3.1) and AMZ-0-89-0 (Appendix 3.2). This is because the ionic radii of Al^{3+} (0.53 Å) and Mg^{2+} (0.65 Å) are significantly smaller than that of La^{3+}, hence the latter cannot dissolve in the former two (which are major components in the supports), hence lanthana is expected to segregate in theses supports.

As seen in Figure 14 the hydrothermal aging of the supports increases the crystallite size of various phases. Lanthana present in binary Al_2O_3 (AMZ-89-0-0) does not segregate. A small growth of 6.7% is observed in the crystallite size of the Al_2O_3 phase. Lanthana is reported to stabilize alumina and retard crystallite growth [32]of γ-Al_2O_3. Thus, the results of the current study are consistent with reports in the literature. This also results in better retention of the surface area during hydrothermal aging. Whereas lanthana in the binary magnesia supports (0-89-0) segregates and grows by

4.6%, and the MgO phase grows by only 3%. Similarly, in binary zirconia, lanthana does not segregate but limits the growth of zirconia to 9.1%. Thus, lanthana appears to retard the hydrothermal sintering of all three binary catalysts. All the binary supports (first three from origin) show low growth (3.0-9.1%) in crystallite size upon hydrothermal aging.

The ternary Al_2O_3-MgO and MgO-ZrO_2 supports which contain magnesia in combination with zirconia or alumina also show low growth (2.7-10.8%). Again, in the Al_2O_3-MgO supports it is the MgO phase that shows a small extent of growth, whereas the Al_2O_3 does not show any increase in crystallite size. Within the ternary Al_2O_3-MgO supports crystallite growth of MgO decreases when the magnesia content increases from 44 to 49 wt% and further to 59 wt% (skewed samples). Spinel $MgAl_2O_4$ is the only phase observed in ternary supports of magnesia and alumina ($MgO/Al_2O_3 \geq 2.53$ molar, AMZ-44-44-0, Appendix 3.3). These samples show good hydrothermal stability (2.7 – 5.0% increase in crystallite size of MgO), whereas the Al_2O_3 phase does not show any growth. This is consistent with the character of spinels [33].

Ternary supports of alumina and zirconia (for example AMZ-39-0-49 or AMZ-29-0-59) show significantly higher growth of ZrO_2 upon aging (ranging from 165.7 to 292.9%). Interestingly the Al_2O_3 phase does not grow. Crystallite growth of ZrO_2 increases as the mole ratio of Al_2O_3/ZrO_2 decreases from 1.204 to 0.604 (i.e., as zirconia increases). AMZ-44-0-44 (Al_2O_3/ZrO_2 = 1.204 mole) which has the lowest zirconia content amongst the ternary Al_2O_3-ZrO_2 series shows significantly lower crystallite growth (13.9%) of zirconia. It is also the only ternary support among the three which also shows an increase in the crystallite size of alumina (20.3%). The remaining two ternary zirconia-alumina supports have Al_2O_3/ZrO_2 ratios of 0.604 and 0.954.

Thus, both magnesia and zirconia retard the crystallite growth of Al_2O_3. The results of change in the microstructure of the supports upon hydrothermal aging show that Al_2O_3-ZrO_2 supports have a smaller surface area and pore volume than Al_2O_3-MgO supports before hydrothermal aging but lose less surface area (Figure 5) and pore volume (Figure 7) upon hydrothermal aging.

In quaternary supports, growth of the zirconia phase increases from 72.5 Å (AMZ-22-44-22) to 241.2 Å (AMZ-22-22-44) as the mole ratio of MgO/ZrO_2 decreases from 5.97 to 1.53. AMZ-44-22-22, which is alumina rich shows crystallite growth of zirconia by 200%. It also shows a small increase in the crystallite size of alumina

(2.4%). The AMZ-22-44-22 (Magnesia-rich support) also shows the significant growth of the MgO phase (44.9%) in addition to the growth of zirconia (72.5%). The zirconia-rich quaternary support AMZ-22-22-44 shows the highest growth of zirconia but does not show alumina or magnesia. It appears these phases exist as a solid solution and zirconia tends to segregate upon hydrothermal aging.

Thus, amongst the calcined supports crystalline γ-Alumina is detected only in binary AMZ-89-0-0. Crystallite size increases by 6.7% upon hydrothermal aging. Al_2O_3 is also observed in ternary AMZ-44-0-44 (Appendix 3.5), and quaternary AMZ-44-22-22 (Appendix 3.6) but only after hydrothermal aging. It is x-ray amorphous in the remaining supports even after hydrothermal aging. Hydrothermal aging increases the crystal size of Al_2O_3 by 20.3% in AMZ-44-0-44, which is significantly larger than in the other two (6.7% in binary Al_2O_3 AMZ-89-0-0 and 2.4% in quaternary AMZ-44-22-22 respectively). Thus, the presence of crystalline Al_2O_3 or its growth is observed only when its content in the supports is ≥44 wt%. The presence of magnesia and zirconia in the quaternary AMZ-44-22-22, and zirconia in the ternary AMZ-44-0-44 supports appear to prevent/contain crystallite growth of alumina.

Amongst the binary supports, MgO (periclase phase) is observed only in binary AMZ-0-89-0 (Appendix 3.2). It grows by 3% upon hydrothermal aging. Growth of MgO is also observed in all three ternary Al_2O_3-MgO catalysts. Interestingly, growth decreases as the content of MgO increases. The trend of decrease is AMZ-44-44-0>AMZ-39-49-0>AMZ-29-59-0. Significant growth of MgO is also observed in quaternary AMZ-22-44-22 (Appendix 3.7). Its crystallite growth is 44.9% upon aging which is attributed to the high molar ratio of MgO/ZrO_2 (5.96). Magnesia forms a complete solid solution with zirconia when MgO/ZrO_2 ≤3.06 molar (ternary support AMZ-0-44-44, quaternary supports AMZ-44-22-22 and AMZ-22-22-44 (Appendix 3.4, 3.6, 3.8 respectively).

ZrO_2 is observed to exist as its tetragonal phase in all the supports containing zirconium. It appears to largely form an amorphous solid solution with both alumina (AMZ-44-0-44, Appendix 3.5) and magnesia (AMZ-0-44-44, Appendix 3.4). Crystallite growth of zirconia is small (13.9 and 10.8% respectively) after hydrothermal aging in these two ternary supports. However, it appears to segregate significantly in all skewed Al_2O_3-ZrO_2 supports and also all three quaternary supports when its content in the support exceeds a nominal 44 wt%.

Thus, it is seen that the formation of solid solutions influences the following properties:

i) Microstructure of the supports: BET-specific surface area of ternary alumina-zirconia supports (AMZ-44-0-44 or AMZ-29-0-59 in Figure 2) is retained, when they are hydrothermally aged at 750°C for 4 hours.

ii) Acid character of these supports: Change from higher to lower acid strength when Al_2O_3 and ZrO_2 are combined in their ternary counterparts. The Al_2O_3-ZrO_2 ternary supports show lower acid strength of the high-temperature peak T2 in NH_3 TPD (Figure 12) when compared with the corresponding binary supports AMZ-0-0-89 (zirconia) and AMZ-89-0-0 (alumina). Similarly, the ternary alumina-zirconia support (AMZ-29-0-59) shows the highest total acidity amongst all the catalysts, whereas the binary zirconia composite AMZ-0-0-89 has high total acidity and alumina support AMZ-89-0-0 has intermediate total acidity (Figure 13). Its total acidity is significantly higher than that of zirconia (which has the second-highest acidity among all the supports). Similarly, the supports which contain zirconia and magnesia with or without alumina (AMZ-0-44-44 or AMZ-22-44-22 or AMZ-22-22-44) (Figure 13) show total acidity which is significantly lower than that of binary ZrO_2 (0-0-89), which has the highest total acidity.

iii) Ternary supports of Magnesia-alumina (example AMZ-39-49-0) also show higher acidity than those of magnesia and zirconia (example AMZ-0-44-44) although binary zirconia (AMZ-0-0-89) has significantly higher acidity than binary samples of magnesia or alumina. These unexpected characteristics (anomalies) are attributed to the formation of amorphous solid solutions which is also supported by observation in P-XRD of these samples. Thus, it is observed that there are significant interaction effects between individual components in the ternary and quaternary supports.

2.3.5: Oxygen Storage Capacity measurements of Supports.

Oxygen mobility is reported to improve catalyst stability by aiding the combustion of carbonaceous deposits [34]. The oxygen storage capacity of composites calcined at 650°C is presented in Figure 15 below.

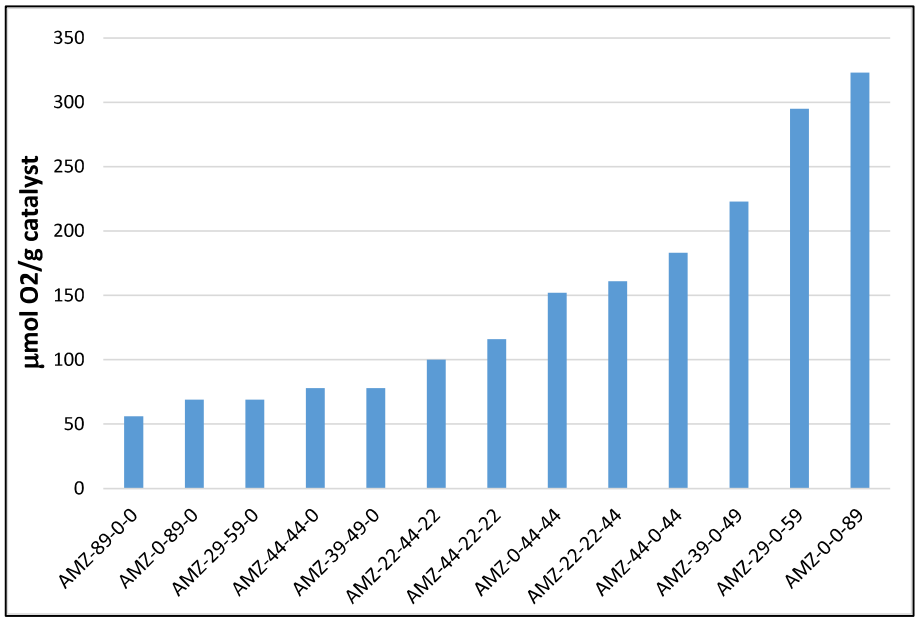

Figure 15: Oxygen storage capacity (OSC) of composites calcined at 650°C.

Ceria is known for its oxygen storage capacity which is important for scavenging coke deposits in catalysts used for steam reforming [35]. OSC was determined by the method of Madier et. al.[36]. This comprises of first reducing the supports with hydrogen and then oxidizing then by pulsing oxygen. After oxidation, carbon monoxide is pulsed to titrate CO to CO_2. The oxygen storage capacity is determined by the amount of carbon dioxide formed. All the supports contain a nominal 5.4% CeO_2. As seen from Figure 15, supports that do not contain ZrO_2 (first five samples towards the origin) show low values of OSC which range from 56-78 µmol O_2/g catalyst. This is attributed to the OSC of Ceria. When ZrO_2 is incorporated into the supports OSC increases significantly from 100 µmol O_2/g for the quaternary AMZ-22-44-22 support to 323 µmol O_2/g for the binary AMZ-0-0-89 support indicating a synergistic effect between ceria and zirconia. Binary zirconia (AMZ-0-0-89) shows the highest OSC amongst the entire series of catalysts studied. This is closely followed by the Al_2O_3-ZrO_2 support with skewed composition and then by the Al_2O_3-ZrO_2 support with balanced composition. Hence, OSC increases with increasing zirconia content when magnesia is absent in the support.

When supports are compared at a constant value of ZrO_2/CeO_2 = 11.5 molar, the trend of OSC is AMZ-44-0-44 (without magnesia)>AMZ-22-22-44 (MgO/ZrO_2 1.53)>AMZ-0-44-44 (MgO/ZrO_2 3.19 molar). Quaternary supports also show a similar trend. They comprise combinations of alumina, magnesia, and zirconia. All three show

lower OSC than ternary supports of alumina-zirconia (which do not contain magnesia). Further, AMZ-22-44-22, which has the highest content of magnesia amongst quaternary supports shows lower OSC than AMZ-44-22-22 (which has similar zirconia content as AMZ 22-44-22). Thus, it appears that the presence of magnesia decreases OSC.

Linear regression of OSC versus ZrO_2/CeO_2 molar ratio up to 15.3 shows a polynomial trend.

$$OSC = 2.38 * (\frac{ZrO}{CeO2})^2 - 30.429 \left(\frac{ZrO_2}{CeO_2}\right) + 203.54 \quad (R^2 = 0.963). \qquad \text{(Equation 2)}$$

Ceria-zirconia binary supports have been studied by Licheng Liu [42] and Suda et.al [43]. Both report that OSC is maximum at ZrO_2/CeO_2 1 ratio (molar). This differs from the observation of the current study where it increases up to a molar ratio of 23. The cause appears to be the presence of other components (alumina, magnesia and lanthana) which can act as spacers/diluents and decrease the proximity between ceria and zirconia. The proximity between the two increases with increasing zirconia content of the support. However, Biswas et.al. [8] have studied 10-40 wt% Ni supported CeO_2, ZrO_2 and mixed oxides of ceria and zirconia with CeO_2/ZrO_2 weight ratio varying from 0.25-4. They have studied the degree of reduction of lattice oxygen of CeO_2. Their results show that the degree of reduction increases from 10.8% in neat CeO_2 to 57% for $Ce_{0.16}Zr_{0.84}O_2$. Thus, their results show a trend similar to that observed in the current study.

2.3.6: Thermogravimetry (DSC-TG) measurements of Supports

Samples of the supports which were dried at 120°C were studied by DSC-TG. The results of these studies are presented in Figure 16. The DSC-TG patterns are provided in Appendix 4

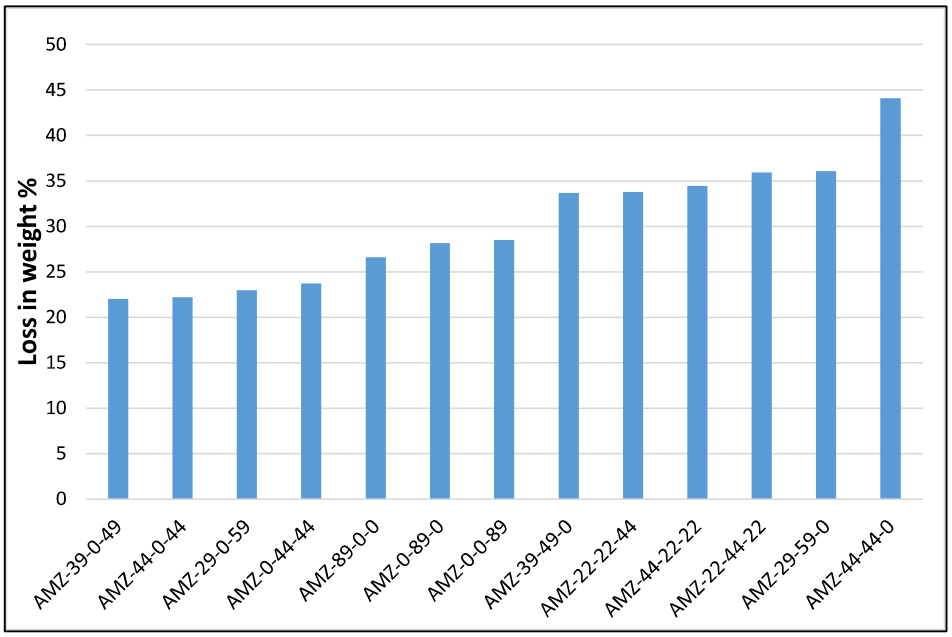

Figure 16: Trend of weight loss in DSC-TG of composites dried at 120°C.

The following distinct trends of weight loss with composition are observed in Figure 16: binary supports of alumina (AMZ-89-0-0), magnesia (AMZ-0-89-0) or zirconia (AMZ-0-0-89) show total weight loss in a narrow band (26.6-28.5 wt%). Amongst these, AMZ-89-0-0 shows a total weight loss of 26.6 wt% at 800°C which is in the ballpark range of what is expected theoretically from the transformation of pseudo-boehmite to alumina (25-28 wt%) as per the stoichiometry shown below. It also includes bonded/intercalated water which is variable in content (not shown in the equation):

$$2\,AlO(OH) = Al_2O_3 + H_2O$$

The binary magnesia support AMZ-0-89-0 shows a total weight loss of 28.2 wt% against 30.9 wt% which is expected theoretically for the conversion of $Mg(OH)_4$ to MgO. Thus, the value is close to theoretical.

The binary zirconia support AMZ-0-0-89 shows a total weight loss of 28.1 wt%. Zirconia can precipitate in the form of zirconium hydroxide ($Zr(OH)_4.nH_2O$) and/or hydrous zirconia ($ZrO_2.nH_2O$)[44]. The structural difference in their tetramers is that the former contains 44 bridging hydroxyls whereas the latter contains only 22 tetramers. The theoretical weight loss of the former is 32 wt% whereas that of the latter is 21.5 wt% [44]. The experimental value 28.1 wt% of binary AMZ-0-0-89 is closer to the

former. Thus, the binary zirconia prepared in the current work is expected to be $Zr(OH)_4.nH_2O$.

The ternary supports however show a different behaviour from the binary supports. They show a broad range of total weight loss ranging between 22.2%-44 wt%. Amongst these, the supports of alumina-magnesia (example AMZ-44-44-0) show total weight loss in the range of 30%-44 wt%, whereas supports of zirconia with either of alumina (example AMZ-44-0-44) or magnesia (AMZ-0-44-44) show significantly lower weight loss (22.1%-23.7 wt%). Thus, the surface of the ternary composites containing zirconia is expected to be much less hydroxylated than those of magnesia-alumina and also the binary composite of zirconia alone (AMZ-0-0-89), which shows a weight loss of 28.1 wt%. Thus, it appears that Zr-O-Me (where Me = Al or Mg) bonds which form by condensation occur through oxolation rather than by olation during precipitation.

It is further observed that the ternary supports with balanced composition show higher weight loss than supports with composition skewed in favour of magnesia or zirconia.

The quaternary supports show total weight loss in the range of 33.7-35.9 wt% which is similar to that of ternary Al_2O_3-MgO supports. The effect of zirconium which lowers the total weight loss in its ternary composites is not observed in the quaternary composites.

It is further seen from Appendix 4.1 to 4.3 that the binary composites of alumina (AMZ-89-0-0) or magnesia (AMZ-0-89-0) show weight loss <3 wt% at temperature 200°C, whereas the binary composite of zirconia (AMZ-0-0-89) shows a weight loss of 9 wt%. This suggests that binary zirconia has significantly more physisorbed water amongst the three samples. This is consistent with its total weight loss which indicates that it is probably $Zr(OH)_4.nH_2O$. These trends are also observed in ternary and quaternary composites containing zirconia.

From the Figures in Appendix 4, it is also seen that:

The binary composites show characteristic DSC peaks such as endothermic peaks at 140°C, 250°C, and 435°C in the case of AMZ-89-0-0 (Appendix 4.1) which are assigned to dehydroxylation and phase transition to gamma-Al_2O_3. A single endothermic peak at 390°C in AMZ-0-89-0 (Appendix 4.2) is assigned to the transition of $Mg(OH)_2$ to MgO. Endothermic peaks at 180°C and 840°C in AMZ-0-0-89

(Appendix 4.3) are assigned to the transition of zirconium hydroxide to ZrO_2 and further transition to polymorphs.

Amongst the ternary composites, the supports of alumina and magnesia, AMZ-44-44-0 (Appendix 4.4), AMZ-39-49-0 (Appendix 4.7) and AMZ-29-59-0 (Appendix 4.8) show DSC pattern which resembles that of binary alumina AMZ-89-0-0 (endotherm at 390°C). Peaks for MgO are conspicuously absent. XRD shows the formation of $MgAl_2O_4$ spinel in all these samples which explains the absence of the endotherm for MgO.

The ternary composites of Al_2O_3-ZrO_2, AMZ-44-0-44, AMZ-39-0-49 and AMZ-29-0-59 (Appendix 4.6 for AMZ-44-0-44 shown as representative), show peaks which are characteristic of binary oxides of alumina and zirconia (endotherms at 77°C -90°C and 250-265°C, exotherm at ~830°C). Zirconia is detected in these samples whereas alumina is not detected by P-XRD which indicates that the alumina is in the form of a solid solution in zirconia. Composite AMZ-0-44-44 (Appendix 4.5) which is a ternary support containing magnesia and zirconia does not show DSC peaks representative of magnesium or zirconium compounds. P-XRD too does not show peaks for MgO in this sample (Appendix 4.4). Only the peak for t-ZrO_2 is observed, thus magnesia exists as a solid solution in zirconia. Gocmez et.al. [46] have prepared solid solutions of magnesia and zirconia by the citrate gel method where the MgO content is varied from 3-90 mol%. They report that ZrO_2 exists in its metastable tetragonal form in samples calcined at 800°C.

The quaternary supports (Appendix 4.10, 4.11 and 4.12) show multiple DSC peaks resembling those of ternary samples. DSC peaks of individual components (alumina, magnesia and zirconia) become evident in these supports when their content increases in the support. Hence, some degree of identity of individual components is retained in these composites despite the formation of solid solutions. Simultaneously, composites AMZ-44-22-22 (MgO/ZrO_2 3.06, Appendix 4.10) and AMZ-22-44-22 (MgO/ZrO_2 6.11 molar, Appendix 4.11) also show a shift of exotherms to lower temperature 440°C and 540°C respectively indicating interaction effects between the individual metal oxides.

2.3.7: Fourier Transform Infra-Red (FTIR) Spectroscopy measurements of Supports

Results of FTIR of relevant uncalcined composites which are dried at 120°C are presented in Appendix 5.

The following inferences can be drawn:

Signals from 3200-4000 cm^{-1} which are attributed to surface hydroxyls [43] in the literature show the following trends: all the binary supports AMZ-89-0-0, AMZ-0-89-0 and AMZ-0-0-89 (Appendix 5.1, 5.2 and 5.3) show this band at 3441-3442 cm^{-1}. The magnesia-containing composite (AMZ-0-89-0, Appendix 5.2) shows an additional band at a higher frequency, 3698 cm^{-1}. This is attributed to the more basic character of bands at lower frequencies [48]. The basic character of AMZ 0-89-0 is also confirmed independently from the results of NH_3 TPD and the decomposition of MBOH reported in this chapter.

The ternary composite of Al_2O_3-ZrO_2, AMZ-44-0-44 (Appendix 5.5) shows the splitting of the hydroxyl band into 3-4 peaks at 3549, 3460 and 3419 cm^{-1} indicating the presence of sites with subtle differences in acidity. This is also reported by H. Knozinger et.al. [48].

All the supports show bands of medium intensity in the frequency range 1632-1633 cm^{-1}. These are assigned to bridged bidentate carbonates [45,46] which are formed due to the adsorption of CO_2 from the atmosphere. Two metal atoms need to be close to each other in order to facilitate this type of bonding. Bands in the region 980-1020 cm^{-1} are also assigned to this species. These are observed in ternary composite AMZ-44-0-44 (Appendix 5.5) and all three quaternary composites (Appendix 5.6 for AMZ-22-44-22 is shown as representative).

Weak bands are observed in the frequency range 1558-1561 cm^{-1} in all the supports. The band in the region 1530-1620 cm^{-1} is attributed to chelating bidentate metal carbonates [49, 52].

The band at 1384 cm^{-1}, is also observed in all the supports. This is attributed to monodentate carbonate [49]. The intensity of this band is strongest in all three binary supports and the ternary support comprising of alumina and magnesia (AMZ-44-44-0) which has balanced composition. The intensity of this band is weak in supports in which magnesium is either absent or present in lower concentrations (for example ternary

AMZ-44-0-44 or quaternary AMZ-22-22-44) which is consistent with decrease in affinity of CO_2 as basicity of the support decreases. This band is bidentate and its relative intensity at 1367 cm^{-1} is higher for the quaternary support AMZ-22-22-44 (Appendix 5.7) which has the highest content of zirconia among the three. Bands are also observed in the region 1054-1070 cm^{-1} for most of the supports. These are attributed to metal carbonate species.

Very weak bands are observed in the region 449-900 cm^{-1} in many of the supports. The band at 448-450 cm^{-1} is prominent in supports containing magnesia and alumina (example Appendix 5.4). This band, which is observed at a higher frequency (458 cm^{-1}) in the binary composite AMZ-0-89-0 (Appendix 5.2) shifts to a lower frequency in ternary Al_2O_3-MgO supports when $MgAl_2O_4$ is formed.

2.3.8: MBOH – Model reaction for chemical characteristic of Supports

The decomposition of 2-methyl-3-butyn-2-ol (MBOH) [40] was first reported by researchers from Rhone Poulenc. It is useful in studying metal oxides for their acid-base characteristic and serves to complement the NH_3 TPD method. It produces equimolar quantities of acetone and acetylene on basic sites, Mbyne (3-methyl-3-buten-1-yne) and prenal (3-methylcrotonaldehyde) on acidic sites and HMB (3-hydroxy-3-methyl-3-butanone) and MiPK (3-methyl-3-butene-2-one) on amphoteric sites. MBOH was procured from Sigma Aldrich.

The results of the conversion of MBOH for binary composites are shown in Figure 17 (a) below.

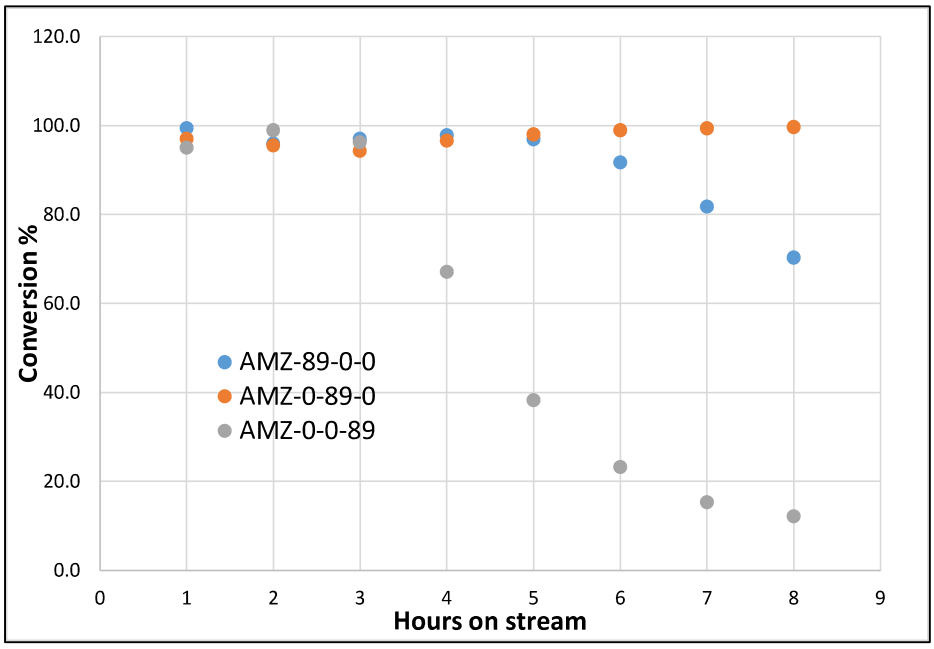

Figure 17(a): MBOH conversion trend of binary composites calcined at 650°C

As seen from Figure 17(a) all three composites show almost complete conversion (>97%) of MBOH initially. However, the composite containing magnesia (AMZ-0-89-0) shows the highest stability followed by the composite containing alumina (AMZ-89-0-0). Whereas the zirconia composite (AMZ-0-0-89) shows rapid deactivation after the 3rd hour on stream. To identify the cause of deactivation the results of the conversion are compared with the total acidity of these composites as determined by NH_3 TPD (refer to Figure 14). Total acidity follows the trend AMZ-0-0-89 > AMZ-89-0-0 > AMZ-0-89-0. Thus, supports with higher acidity deactivate faster, clearly showing that deactivation is influenced by the acidity of the supports.

The trend of time on stream conversion of MBOH of ternary and quaternary composites is shown in Figures 17 (b) and 17 (c) below respectively. As seen from these figures all the ternary supports show some deactivation with time on stream. As seen from Figure 17 (b), the ternary composites which comprise alumina and magnesia show almost complete conversion initially and much slower deactivation than composites comprising alumina and zirconia or zirconia and magnesia. The ternary alumina-magnesia supports (with balanced or skewed composition) show high initial activity with slow deactivation with time on stream. Between ternary composites of alumina-zirconia and zirconia-magnesia, the latter shows lower initial conversion but significantly slower deactivation than the former.

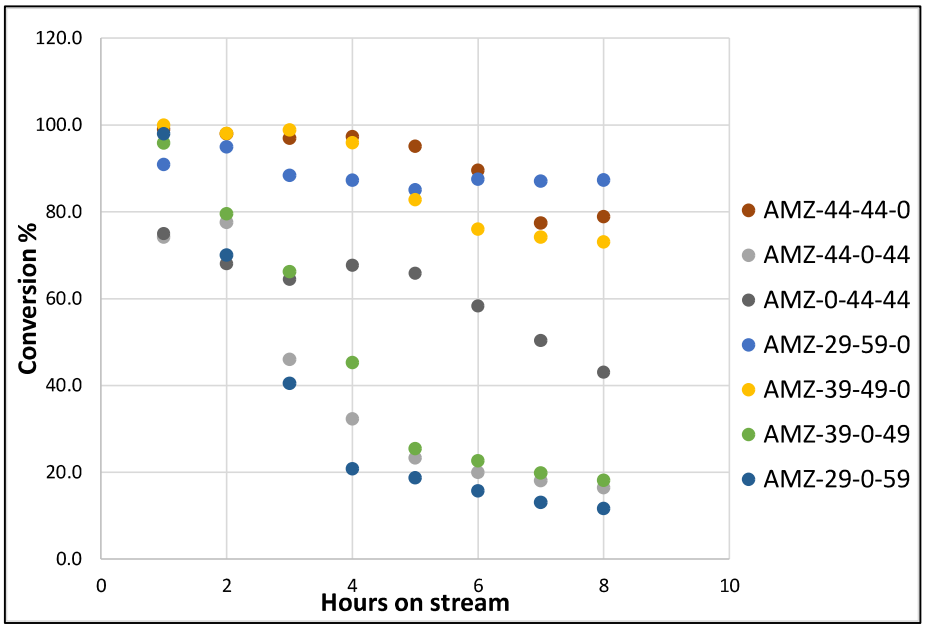

Figure 17(b): MBOH conversion trend of ternary composites calcined at 650°C

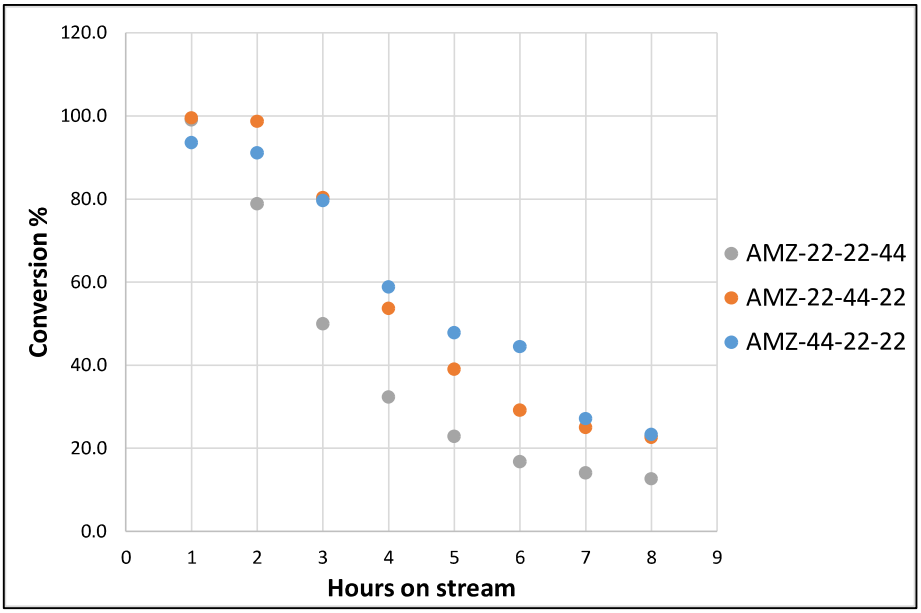

Figure 17(c): MBOH conversion trend of quaternary composites calcined at 650°C.

The trend of conversion with time on stream of the quaternary composites is shown in Figure 17 (c) above. As seen from this Figure all three supports show similar initial activity and deactivation. However, the zirconia-rich support (AMZ-22-22-44) shows relatively faster deactivation than the alumina or magnesia-rich supports. The benefit of magnesia in slowing down deactivation in binary and ternary composites is not as significant in the quaternary composite. The deactivation constants are presented in Figure 21.

Acetone and acetylene are reported to form in equimolar quantities on basic sites of the support. The time on stream trends of selectivity of the composites calcined at 650°C to these products is shown in Figures 18(a) to 18 (d) below. Since these products are formed in equimolar proportions only the selectivity of acetone is shown in Figure 18 (a).

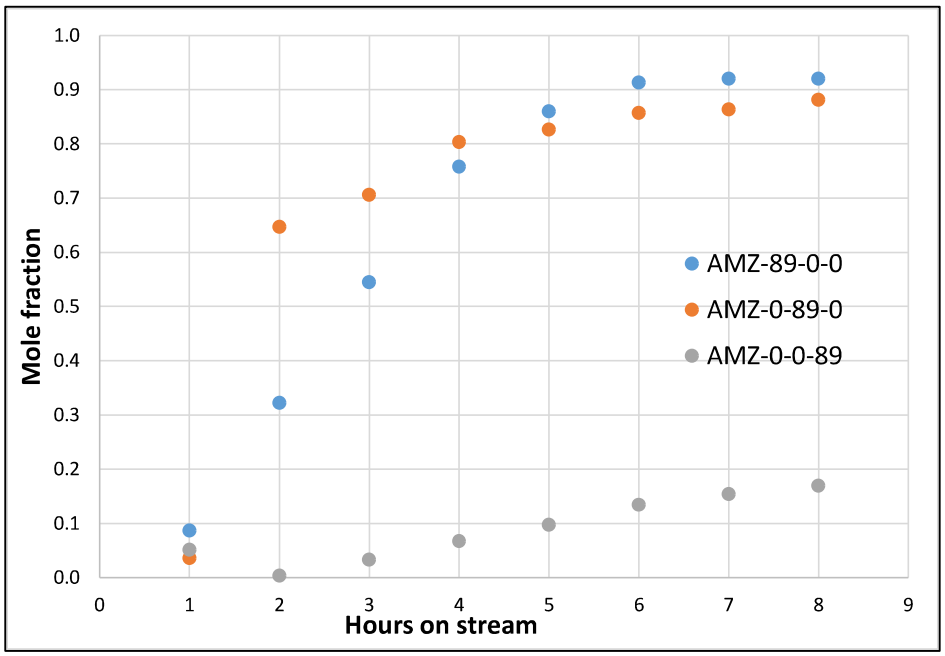

Figure 18(a): Selectivity of binary composites to acetone.

As seen from the trends in Figure 18 (a) all three binary composites show comparable selectivity to acetone initially. The selectivity is <10 mole%. At the 2nd hour on stream, there is significant differentiation in selectivity between the three supports. The magnesia support shows significantly higher selectivity followed by alumina and then zirconia support. The selectivity of the alumina support catches up with that of the magnesia support by the 4th hour on stream and both stabilize at about 90% at the 6th hour on stream. However, the steady-state selectivity of alumina and magnesia supports is significantly higher than that of zirconia support (which is just 15 mole%).

The selectivity of ternary composites to acetone is shown in Figure 18 (b).

As seen from Figure 18 (b) the selectivity stabilizes by 2 hours on stream, much earlier than for binary supports. The composites of alumina and magnesia show the highest selectivity to acetone and acetylene (>92-99%) amongst the ternary supports which indicates their basic character. The ternary composite of magnesia and zirconia (AMZ-0-44-44) follows the alumina-magnesia supports with selectivity stabilizing at

about 87-88%. Ternary composites of alumina-zirconia show the lowest selectivity to acetone and acetylene (40-55%) indicating amphoteric character. Thus, the trend is similar to that of the binary composites in the sense that magnesia favors the formation of acetone relative to zirconia.

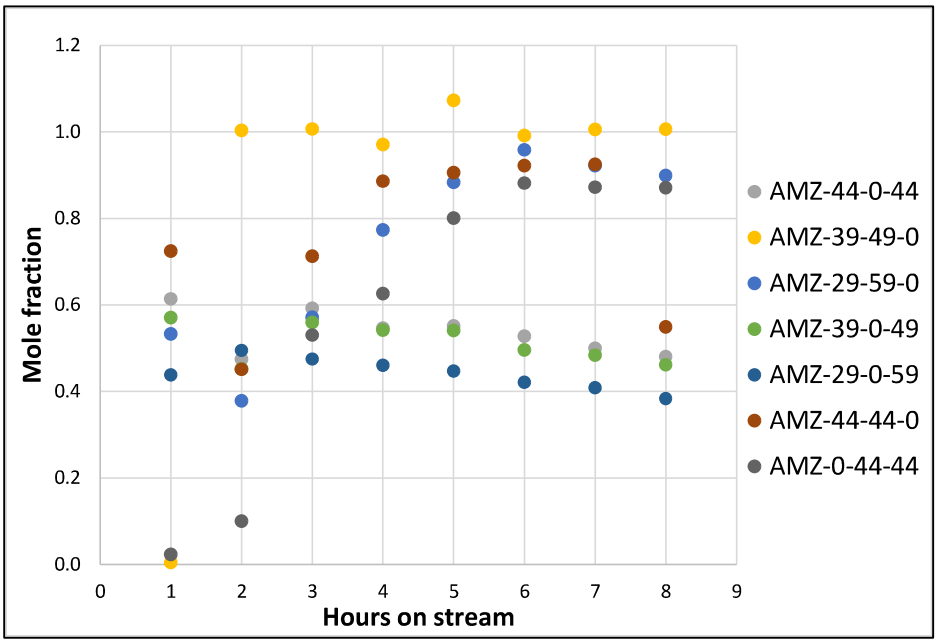

Figure 18(b): Selectivity of ternary composites to acetone and acetylene

The selectivity of quaternary composites to acetone is shown in Figure 18 (c) below.

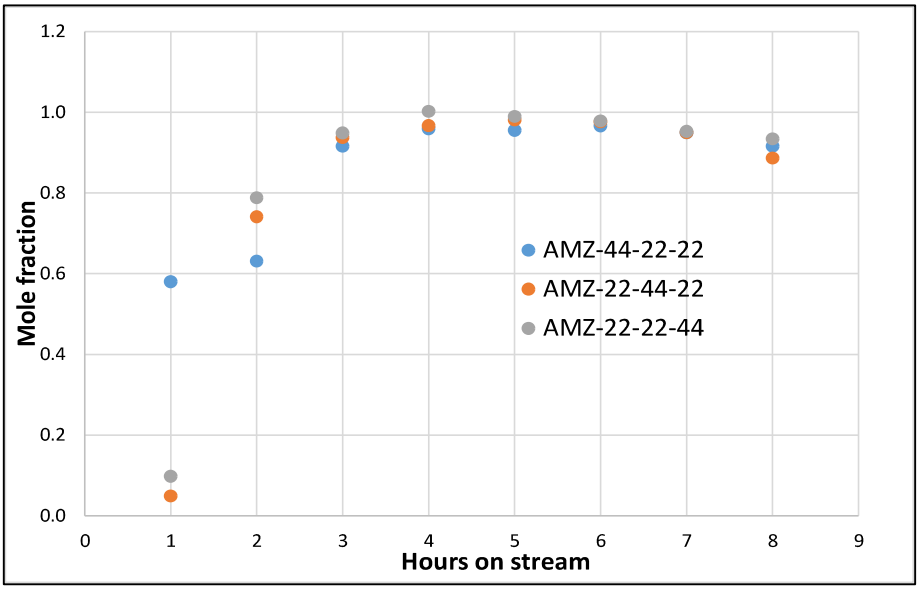

Figure 18(c): Selectivity of quaternary composites to acetone and acetylene

Comparing the trend in Figure 18(c) with those in Figure 18 (a) and 18 (b), it is seen that the distinction which is based on composition in binary and ternary supports is completely lost in quaternary supports and all three composites show similar selectivity to acetone and acetylene. These composites are predominantly basic because they present acetone selectivity close to 99%.

The average value of selectivity to acetone which is taken from the 4th to 8th hour on stream after the conversion had fairly stabilized is compiled in Figure 18 (d) below.

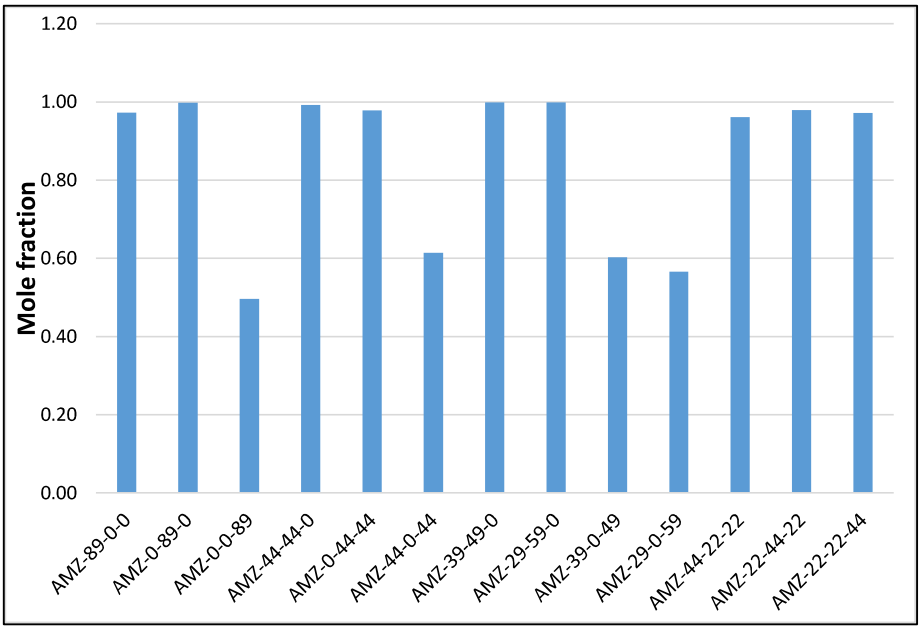

Figure 18(d): Trend of average selectivity to acetone of all the composite samples.

As seen from the data in Figure 18 (d) above the binary alumina support AMZ-89-0-0 which contains alumina, lanthana and ceria shows predominantly basic character.

Composites that do not contain zirconia (viz. ternary composites of alumina-magnesia), and those which contain magnesia with zirconia (AMZ-0-44-44) show predominantly basic character with acetone selectivity exceeding 96%. The binary support of zirconia (AMZ-0-0-89) and all its ternary composites with alumina irrespective of whether the composition is balanced or skewed (AMZ-39-0-49, AMZ-29-0-59, AMZ-44-0-44) show lower selectivity (49%-60%) to acetone, hence indicating lower basicity. Thus, the inclusion of zirconia in the support partially offsets basic character in ternary supports. However, although zirconia is present in quaternary

supports, they present basic character with selectivity to acetone exceeding 95%. Thus, even 22 wt% magnesia gives significant basic character to the supports.

The time on-stream trend of the supports for selectivity to Mbyne, which is formed on acidic sites, is shown in Figures 19 (a) to 19 (c).

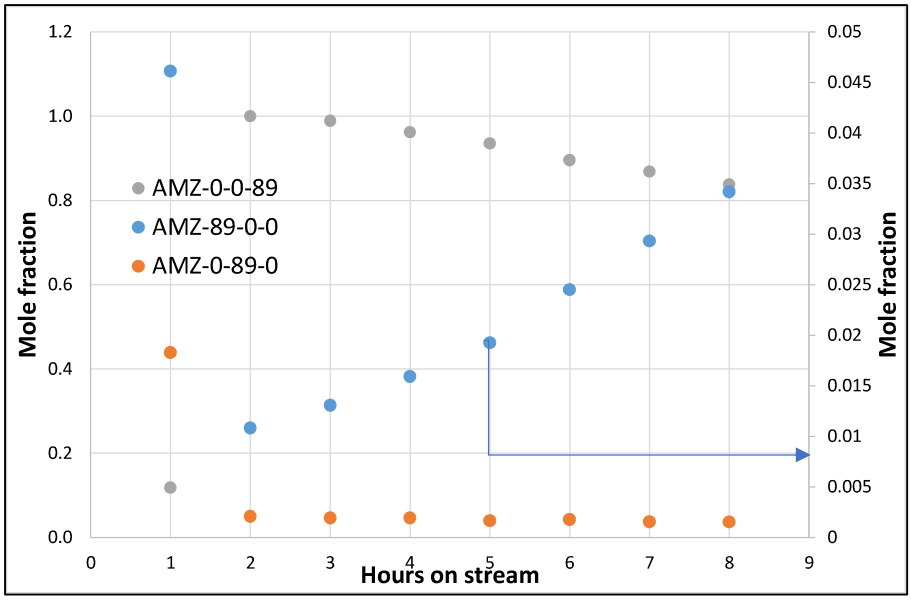

Figure 19(a): Selectivity of binary composites to Mbyne

As seen from the trend in Figure 19 (a), the binary magnesia composite (AMZ-0-89-0) shows very low to negligible selectivity to Mbyne (<1 mol%). The binary alumina composite (AMZ-89-0-0) shows a clear increasing trend while the zirconia composite (AMZ-0-0-89) shows a decreasing trend with time on stream. Between the two the zirconia composite shows an acidic character with selectivity close to 100%. Whereas the alumina composite shows low acidity which gradually increases with time on stream.

Figure 19 (b) shows the time-on-stream trend of selectivity of ternary composites to Mbyne.

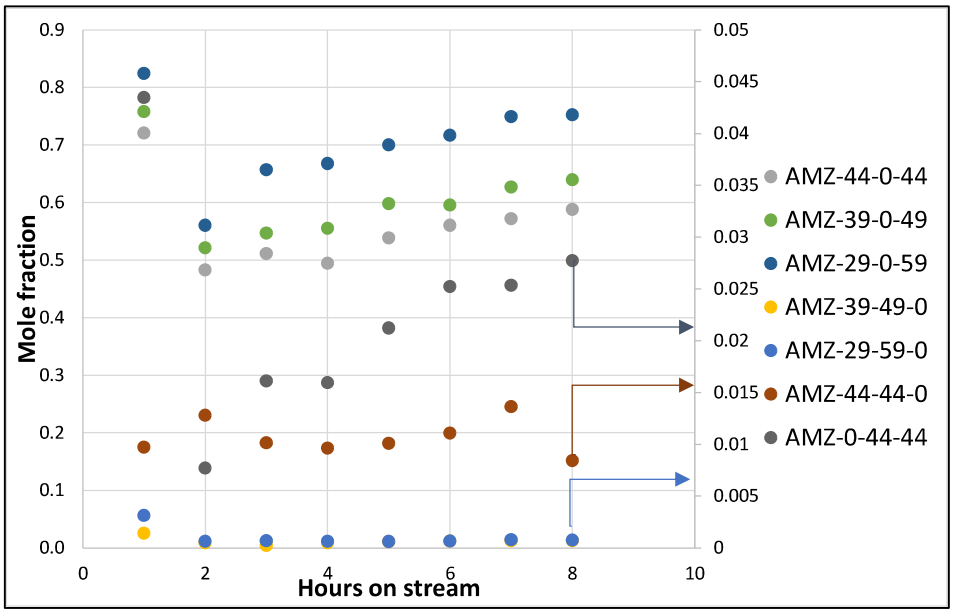

Figure 19(b): Selectivity of ternary composites to Mbyne

As seen in Figure 19 (b), all the ternary alumina-zirconia composites show high selectivity to Mbyne. Within the alumina-zirconia series, the selectivity to Mbyne increases with increasing zirconia content of the support. The trend is AMZ-44-0-44 (balanced composition) < AMZ-39-0-49 (skewed) < AMZ-29-0-59 (skewed). Selectivity of Mbyne increases from about 55% to 63% to 75%. The ternary support of magnesia-zirconia with balanced composition follows the alumina-zirconia supports with stabilized selectivity to Mbyne of 2.5 mol%. The selectivity is observed to increase gradually with time on stream for these supports. Thus, the presence of magnesia drastically decreases acidity (of zirconia). The alumina-magnesia ternary composites show still lower selectivity to Mbyne than the magnesia-zirconia support. Within the alumina-magnesia ternary supports the one with balanced composition, which contains the least magnesia shows relatively higher selectivity to Mbyne whereas both the alumina-magnesia supports with skewed composition show trace selectivity to Mbyne. The selectivity of the alumina-magnesia supports remains steady with time on stream. While the trends are in line with the trend of binary zirconia composite, the acidic character of alumina is not evident in the alumina-magnesia ternary composites possibly due to formation of $MgAl_2O_4$ spinel. Thus, magnesia completely smothers acidic and amphoteric character of zirconia and alumina.

The time on stream trends of quaternary composites for the formation of Mbyne is shown in Figure 19 (c).

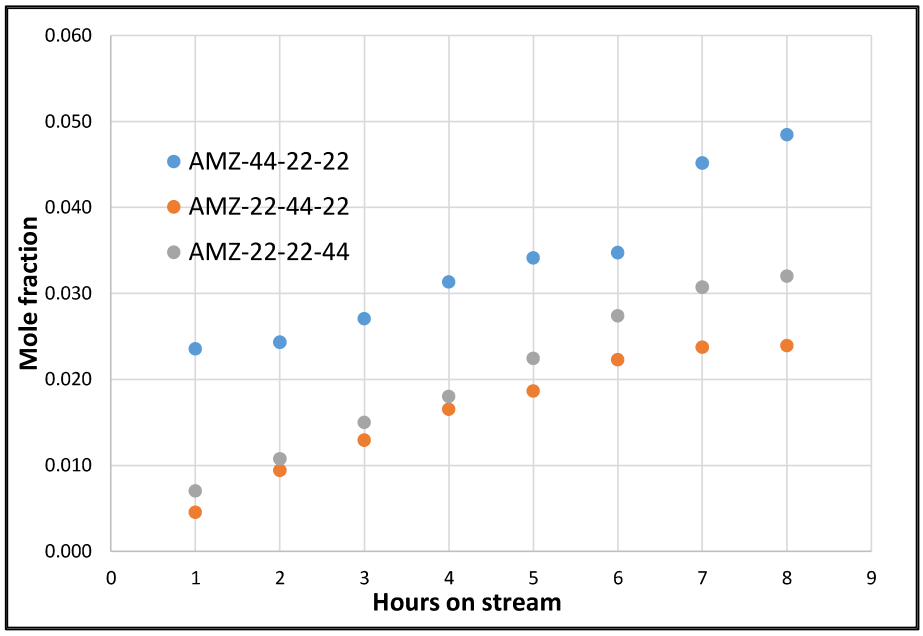

Figure 19(c): Selectivity of quaternary composites to Mbyne

As seen from trends in Figure 19 (c), the acidic character of zirconia and alumina is significantly subdued in quaternary composites too. Selectivity values range from 0.5 to 2.4 mol% initially and 2.4 to 4.8 mol % at the 8th hour on stream. The trend is AMZ-44-22-22 > AMZ-22-22-44 > AMZ-22-44-22. Composite with higher alumina content show greater selectivity to Mbyne than that with higher zirconia content followed by higher magnesia content. Thus, unlike selectivity to acetone, some differentiation is evident between the quaternary supports for selectivity to Mbyne. Further, the selectivity of all three quaternary supports shows an increase in selectivity to Mbyne with time on stream, which is similar to the behaviour of the binary alumina support.

The average selectivity of all the composites to Mbyne is presented in Figure 19 (d) below.

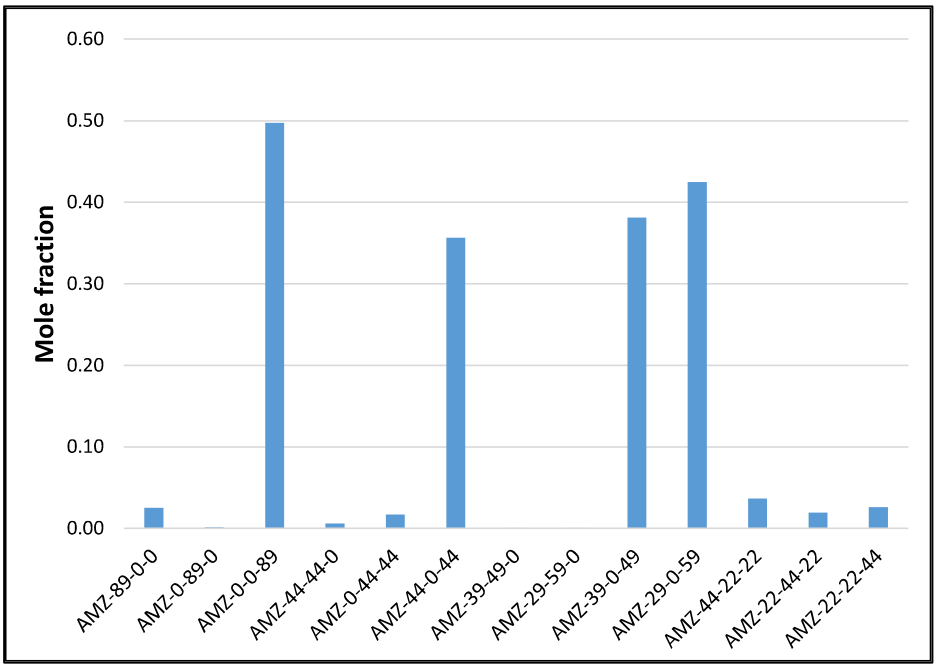

Figure 19(d): Average selectivity of all the composites to Mbyne

As seen from Figure 19 (d) binary composite of zirconia and ternary alumina-zirconia composites stand out in selectivity to Mbyne, indicating acidic character. Binary zirconia shows higher selectivity than ternary alumina-zirconia composites. The remaining composites show very low selectivity to Mbyne.

The trend in MByne in (Figure 19 (a)) is opposite to that of the trends of acetone (Figure 18 (a)). The binary zirconia support AMZ-0-0-89, (which presents the highest total acidity amongst the supports by NH_3 TPD) and its ternary composites with alumina (Figure 19 b) show significantly higher selectivity to MByne (36-50%). The high selectivity is attributed to the higher acidity of these supports. Further, it is observed that the selectivity of the ternary supports of alumina and zirconia to Mbyne increases as the mole ratio ZrO_2/Al_2O_3 increases from 0.83 to 1.66. Thus, increasing the zirconia content of the support in ternary Al-Zr supports increases acid character. All supports which contain magnesia show very low MByne. This is attributed to the low acidity of magnesia. Thus, it is seen that the trends of product selectivity for the decomposition of MBOH correlate well with the trends of total acidity as determined by NH_3 TPD (Figure 13).

The average selectivity to MiPK is shown in Figure 20 below. The trend for selectivity to MiPK is similar to that of Mbyne. However, in contrast to the selectivity of Mbyne, the ternary alumina-zirconia composites show higher selectivity than the

binary zirconia composite. The magnesia-zirconia ternary composite shows higher selectivity to MiPK than the remaining binary, ternary Al-Mg and quaternary composites.

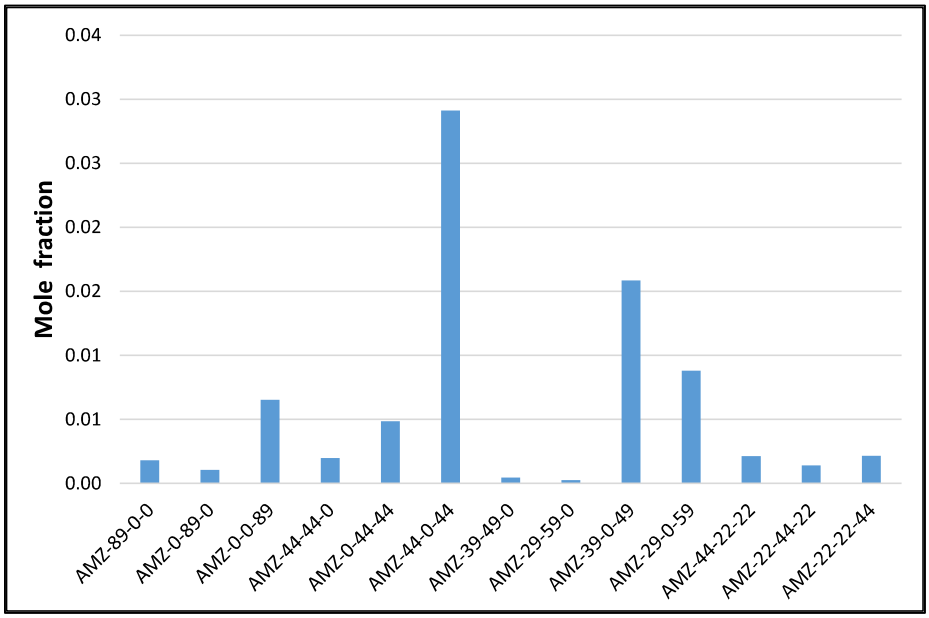

Figure 20: Average selectivity of all the composites to MiPK

Since the catalysts present deactivation (Figures 17 a, b and c), decay constants were determined using a simple power law model. These are presented in Figure 21 below.

As seen from Figure 21, the binary composite AMZ-0-89-0 which contains magnesia and rare earths (La and Ce) presents the slowest deactivation, followed by its ternary composites with alumina and then zirconia. Binary composite AMZ-0-0-89 which contains zirconia and rare earths shows the fastest deactivation. Composite AMZ-89-0-0 which contains alumina and rare earths shows deactivation faster than most of its ternary composites with magnesia, except AMZ-39-49-0.

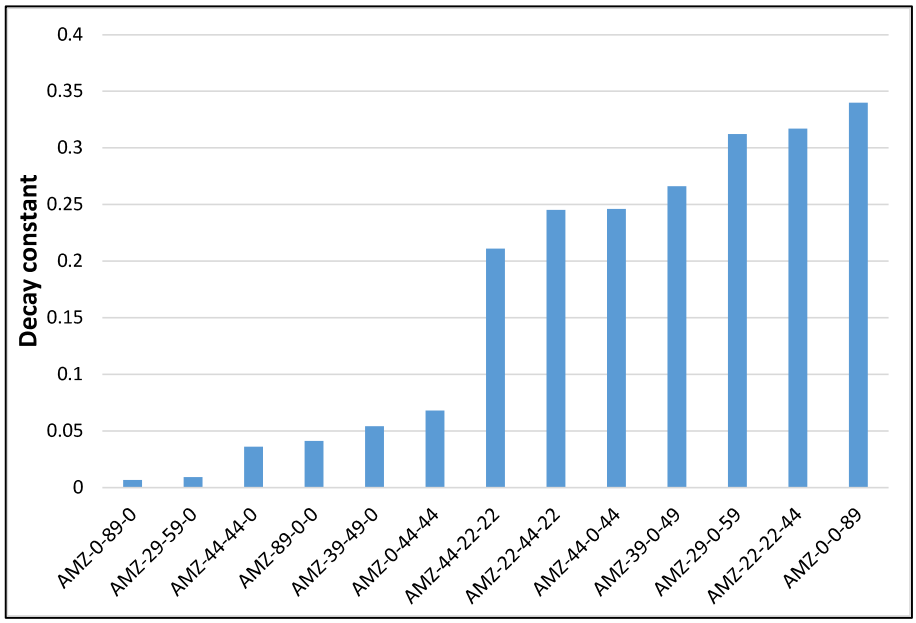

Figure 21: Decay constants of composites for decomposition of MBOH

All the ternary supports which contain zirconia, and all the quaternary composites (which also contain zirconia) deactivate much faster than the remaining supports. Further, the rate of deactivation increases with increasing content of zirconia. The ternary support of magnesia and zirconia (AMZ-0-44-44) presents the slowest deactivation amongst the composites which contain zirconia which appears to be due to the influence of magnesia. Thus, magnesia and zirconia largely influence deactivation behaviour in contrasting ways. Supports that contain zirconia, which is more acidic in character (as seen from NH_3-TPD studies) deactivate much faster than supports which contain magnesia, which is basic in character.

The fractional compositions of alumina, magnesia and zirconia of the supports are plotted in Figure 22 in order of increasing deactivation for decomposition of MBOH along the X axis.

As seen from this Figure, magnesia is effective in containing deactivation (six composites closest to origin). But this is clearly offset by the presence of zirconia in the remaining supports. 0.71-0.76 mole fraction magnesia shows significantly slower deactivation in ternary supports AMZ-44-44-0, AMZ-39-49-0 and AMZ-0-44-44 whereas 0.73 mole fraction still results in significantly higher deactivation when zirconia is present in quaternary support AMZ-22-44-22. Increasing zirconia to 0.48-mole fraction further speeds up deactivation in AMZ-22-22-44. The cause for deactivation is thus clearly related to the acidic behavior of zirconia.

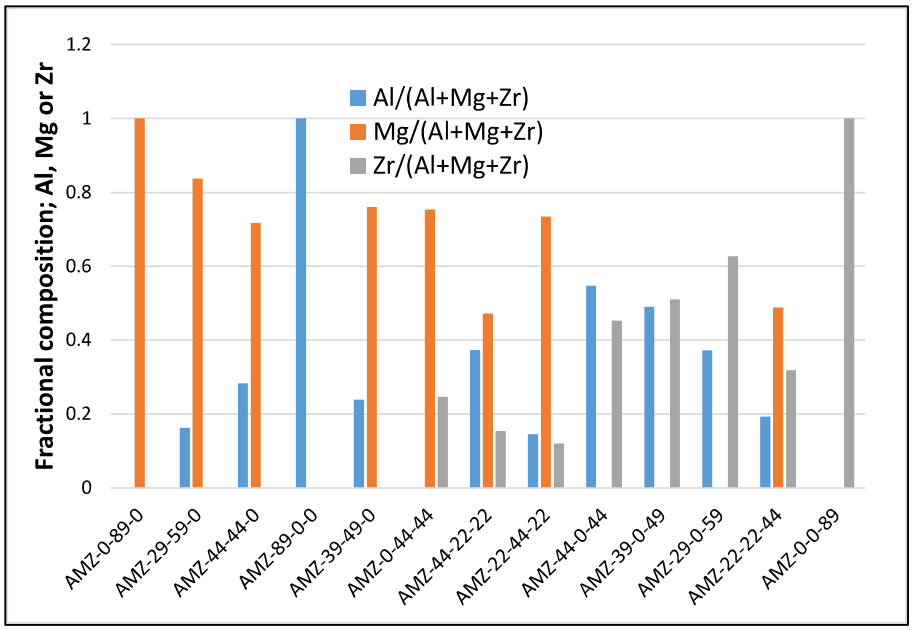

Figure 22: Fractional molar compositions of composites plotted as increasing deactivation for MBOH conversion along X axis.

2.4: Conclusions

Thirteen multi-component composites consisting of rare earths lanthana and ceria of fixed composition and alumina, magnesia and zirconia of variable compositions are prepared and characterized. Binary, ternary, and quaternary compositions are studied. Balanced and skewed compositions are studied in Al-Mg and Al-Zr ternary supports. The supports are extensively characterized.

The Alumina content of the support influences the BET-specific surface area and pore volume of the supports linearly. It also influences the type of hysteresis in N_2 physisorption measurements. Including magnesia and zirconia with alumina decreases specific surface area relative to neat alumina. As seen in the next chapter specific surface area of the support influences the dispersion of Ni in supported catalysts.

The inclusion of zirconia in the support formulations imparts hydrothermal stability which manifests as a lower loss of surface area relative to neat alumina in hydrothermal aging. Whereas ternary Al-Mg shows an opposite trend. This is attributed to the formation of $MgAl_2O_4$ and Zirconia-alumina solid solution as evidenced by XRD. The addition of magnesia or zirconia to alumina also decreases pore volume profoundly. Zirconia shows a larger decrease than magnesia. Overall ternary supports containing zirconia show a smaller decrease in pore volume after hydrothermal aging than those

containing magnesia. Solid solutions result in unexpected trends of acidity of the composites.

The conditions of co-precipitation used in this study result in mesoporous materials. Combining Al with Mg or Zr in ternary supports or combining all three in quaternary catalysts changes pore size distribution from unimodal to bimodal indicating that some characteristic of the monocomponent material is retained in the ternary and quaternary supports. Quaternary supports show the largest pore size amongst the samples.

Supports containing magnesia show lower total acidity compared to zirconia-containing supports which is expected because Mg is an alkaline earth element. Magnesia and zirconia influence acidity in contrasting ways. Thus, the acidity of alumina can be tuned either way by introducing Mg or Zr with it. The ternary supports show unexpected trends of acid strength which are attributed to the formation of spinel (MgO-containing) or solid solutions (zirconia-containing). Acidity determined by the decomposition of MBOH correlates with that determined by NH_3-TPD. The former provides additional information regarding the amphoteric behaviour of the supports. Solid solutions result in unexpected trends of acidity of the composites. Magnesia and zirconia influence acidity in contrasting ways. Supports with higher acidity deactivate faster in the decomposition of MBOH.

Results of XRD confirm the formation of $MgAl_2O_4$ and indicate the formation of largely amorphous zirconia alumina solid solutions. Lanthana and zirconia segregate upon hydrothermal aging due to their larger ionic radii. Zirconia lends better hydrothermal stability to alumina than magnesia in terms of surface area retention. Magnesia and zirconia retard the crystallite growth of alumina in ternary and quaternary supports, thereby imparting hydrothermal stability. It is observed in later chapters that acidity has a strong influence on the catalyst activity and deactivation in ESR (ethanol steam reforming) and EDR (ethanol dry reforming)

The formation of spinels and solid solutions clearly influences the microstructure and acidity of the ternary and quaternary supports.

Zirconia enhances the OSC (oxygen storage capacity) of the support significantly in a linear manner. It augments the OSC of ceria which is present at a nominal 5.5wt % concentration in all the supports. However, magnesia decreases OSC to a small extent.

DSC-TG indicates that zirconia exists as its hydroxide in as-synthesized catalysts. Significant changes are seen in DSC and thermogravimetry trends of multi-component ternary and quaternary supports which indicate the formation of solid solution.

FTIR indicates the presence of surface hydroxyls with subtle differences in acidity as well as the presence of different metal carbonate species due to the adsorption of CO_2.

Microstructure, acid-base character, hydrothermal stability and oxygen storage capacity are correlated with the chemical composition of the composites. Interaction effects between individual components are determined and highlighted. These characteristics are correlated with properties of supported Ni catalysts in chapter 3 and eventually with trends of performance for steam reforming and dry reforming of ethanol in chapters 4 and 5 respectively.

In summary, microstructure, acid-base character, hydrothermal stability, and oxygen storage capacity are correlated with the chemical composition of the composites. Interaction effects between individual components are determined and highlighted. The data is expected to be useful for their selection in reactions such as steam reforming or three-way catalysis.

References

1. N. R. Gard, Nitrogen; 93 (1966); 25.
2. W. Whittenberger and P. W. Farnell, 'Foil Supported Catalysts Deliver High Performance in Steam Reformers', International Methanol Technology Operators Forum (IMTOF), London, UK, 7^{th}–10^{th} June 2015.
3. B. Roy, U. Martinez, K. Loganathan, A.K. Datye, C.A. Leclerc; Effect of preparation methods on the performance of Ni/Al_2O_3 catalysts for aqueous-phase reforming of ethanol: part I-catalytic activity; International Journal of Hydrogen Energy; 37 (2012); 8143-8153.
4. Zahira Yaakob, Ahmed Bshish, Ali Ebshish, Siti Masrinda Tasirin and Fatah H. Alhasan; Hydrogen production by steam reforming of ethanol over Nickel catalysts supported on sol-gel made alumina: Influence of calcination temperature on supports; Materials; 6 (2013); 2229-2239.
5. F. Frusteri, S. Freni, V. Chiodo, L.Spadaro, G. Bonura and S. Cavallaro; Potassium improved stability of Ni/MgO in the steam reforming of ethanol

for the production of hydrogen for MCFC; Journal of Power sources; 132 (2004); 139-144.

6. Gleicielle T. Wurzler, Raimundo C. Rabelo-Neto, Lisiane V. Mattos, Marco A. Fraga, Fabio B. Noronha; Steam reforming of ethanol for hydrogen production over MgO-supported Ni-based catalysts; Applied Catalysis A: General; 518 (2016); 115-128.
7. F. Frusteri, S. Freni, V. Chiodo, S. Donato, G. Bonura, S. Cavallaro; Steam and auto-thermal reforming of bio-ethanol over MgO and CeO_2 Ni supported catalysts; International Journal of Hydrogen Energy; 31(2006); 2193-2199.
8. Prakash Biswas and Deepak Kunzru; Steam reforming of ethanol for the production of hydrogen over Ni/CeO_2-ZrO_2 catalyst: Effect of support and metal loading; International Journal of Hydrogen Energy; 32, (2007); 969-980.
9. Vincenzo Palma, Filomena Castaldo, Concetta Ruocco, Paolo Ciambelli, Gaetano Iaquaniello; Low temperature-ethanol steam reforming over Ni-based catalysts supported on CeO_2; Journal of Power Technologies; 95(1), (2015); 54-66.
10. Liu Qihai, Liu Zili, Zhou Xinhua, L I Cuijin, Ding Jiao; Hydrogen production by steam reforming of ethanol over copper doped Ni/CeO_2 catalysts. Journal of rare earths; 29 (9), (2011); 872.
11. Shuirong Li, Chengxi Zhang, Zhiqi Huang, Gaowei Wu and Jinlong Gong; A Ni@ZrO_2 nanocomposite for ethanol steam reforming: enhanced stability via strong metal-oxide interaction; Chem. Commun; 49 (2013); 4226-4228.
12. R. Padilla, M. Benito, L. Rodrigues, A. Serrano, G. Munaz and L. Daza; Nickel and cobalt as active phase on supported zirconia catalysts for bio-ethanol reforming: Influence of the reaction mechanism on catalysts performance; International Journal of Hydrogen Energy; 35 (2010); 8921-8928.
13. M. Benito, R. Padilla, L. Rodriguez, J.L. Sanz and L. Daza; Zirconia supported catalyst for bioethanol steam reforming: Effect of active phase and zirconia structure; Journal of Power Sources; 169 (2007); 167-176.
14. Jyong-Yue Liu, Chia-Chan Lee, Chi-Han Wang, Chuin-Tih Yeh, Chen-Bin Wang; Application of Nickel-lanthanum composite oxide on the steam

reforming of ethanol to produce hydrogen; International Journal of Hydrogen Energy; 35 (2010); 4069-4075.

15. Raul Carrera Cerritos, Rosalba Fluentes Ramirez, Alberto F. Aguilera Alvardo, J. Merced Martinez Rosales, Tomas Viveros Garcia and Ignacio R. Galindo Esquivel; Steam reforming of ethanol over Ni/Al_2O_3-La_2O_3 catalysts synthesized by sol-gel; I&EC Research; 50 (2011); 2576-2584.
16. Paula Osorio-Vargas, Cristian H Campos, Rufino M Navarro, Jose L. G. Fierro; Improved ethanol steam reforming on Rh/Al_2O_3 catalysts doped with CeO_2 or/and La_2O_3: influence in reaction pathways including coke formation; Applied Catalysis A: General; 505 (2015); 159-172.
17. Paula Osorio-Vargas, Nicolas A. Flores-Gonzalez, Rufino M. Navarro, Jose L. G. Fierro, Cristian H. Campos, Patricio Reyes; Improved stability of Ni/Al_2O_3 catalysts by effect of promoters (La_2O_3, CeO_2) for ethanol steam-reforming reaction; Catalysis Today; 259 (1), (2016); 27-38.
18. Mahadi B. Bahari, Boon Chin Goo, Thong L.M. Pham, Tan Ji Siang, Huong T. Danh, Narul Ainirazali, Dai-Viet N. Vo; Hydrogen-rich syngas production from ethanol dry reforming on La-doped Ni/Al_2O_3 catalysts: Effect of promoter loading; Procedia Engineering; 148 (2016); 654-66.
19. Jose Antonio Torres, Jordi Llorca, Albert Casanovas, Montserrat Dominguez, Joan Salvado, Daniel Montane; Steam reforming of ethanol at moderate temperature: Multifactorial design analysis of Ni/La_2O_3-Al_2O_3, and Fe- and Mn-promoted Co/ZnO catalysts; Journal of Power Sources; 169 (2007); 158-166.
20. Mahadi B. Bahari, Nguyen Huu Phuc, Bawadi Adbullah, Feraih Alenazey, dai-Viet N. Vo.; Ethanol dry reforming for syngas production over Ce-promoted Ni/Al_2O_3 catalyst; Journal of Environmental Chemical Engineering; 4 (2016); 4830-4838.
21. Tatiana de Freitas Silva, Joelmir Augusto Costa Dias, Cristhiane Guinaraes Maciel and Jose Mansur Assaf; Ni/Al_2O_3 catalysts: effects of promoters Ce, La and Zr on the methane steam reforming and oxidative reforming reactions; Catalysis Science & Technology; 3 (2013); 635-643.
22. M.C. Sanchez-Sanchez, R.M. Navarro, J.L.G. Fierro; Ethanol steam reforming over Ni/M_xO_y-Al_2O_3 (M=Ce, La, Zr, Mg) catalysts: Influence of

support on the hydrogen production; International Journal of Hydrogen Energy; 32 (2007); 1462-1471.

23. A.J. Vizcaino, P. Arena, G. Baronetti, A. Carrero, J.A. Calles, M.A. Laborde and N. Amadeo; Ethanol steam reforming on Ni/Al_2O_3 catalysts: Effect of Mg addition; International Journal of Hydrogen Energy; 33 (2008); 3489-3492.
24. Hyun-Seog Roh, Yong Wang, David L. King, Alexandru Platon and Ya-Huei Chin; Low temperature and H_2 selective catalysts for ethanol steam reforming; Catalysis Letters; 108 (2006); 15-19.
25. Evandro Brum Pereira, Pilar Ramirez de la Piscina, Salvador Marti, Narcis Homs; H_2 production by oxidative steam reforming of ethanol over K promoted $Co-Rh/CeO_2-ZrO_2$ catalysts; Energy Environmental Science; 3 (2010); 487-493.
26. Prakash Biswas and Deepak Kunzru; Steam reforming of ethanol on $Ni-CeO_2-ZrO_2$ catalysts: Effect of doping with Copper, cobalt and calcium; Catalysis Letters; 118 (1), (2007);, 36-49.
27. Jorge D.A. Bellido, Eurico Y. Tanabe, Elisabete M. Assaf; Carbon dioxide reforming of ethanol over $Ni/Y_2O_3-ZrO_2$ catalysts; Applied Catalysis B: Environmental; 90, (2009); 485-488.
28. Nicolas Bespalko, Anne-Cecil Roger and Juan Bussi; Comparative study of NiLaZr and CoLaZr catalysts for hydrogen production by ethanol steam reforming: effect of CO_2 injection to the gas reactants, evidence of Rh role as a promoter; Applied Catalysis A: General; 407 (2011); 204-210.
29. Seung Ju Han, Yongju Bang, Jeong Gil Seo, Jaekyeong Yoo, In Kyu Song; Hydrogen production by steam reforming of ethanol over mesoporous $N-=Al_2O_3-ZrO_2$ xerogel catalysts: effect of Zr/Al molar ratio; International Journal of Hydrogen Energy; 38 (2013); 1376-1383.
30. Agustin E. Galetti, Marianna N. Barroso, Manuel F. Gomez, Luis A, Arrua, Antonia Monzon, M. Cristina Abello; Promotion of $Ni/MgAl_2O_4$ catalysts with rare earths for the ethanol steam reforming reaction, Catalysis Letter; 142 (2012); 1461-1469.
31. Ji Hwan Song, Seung Ju Han, Jaekyeong Yoo, Seungwon Park, Do Heui Kim, In Kyu Song; Hydrogen production by steam reforming of ethanol over $Ni-Sr-Al_2O_3-ZrO_2$ aerogel catalyst; Journal of Molecular Catalysis A: Chemical; 424 (2016); 342-350.

32. Ketan Patel, Victoria Blair, Justin Douglas, Qilin Dai, Yaohua Liu, Shenqiang Ren & Raymond Brennan; Structural effects of lanthanide dopants on alumina; (Nature) Scientific Reports; 7 (2017).
33. M.A Sainz, A.D Mazzoni, E.F Aglietti, A Caballero; Thermochemical stability of spines ($MgO.Al_2O_3$) under strong reducing conditions; Materials Chemistry and Physics; 86(2-3), (2004); 399-408.
34. Lisiane V. Mattos, Gary Jacobs, Burtron H. Davis, Fabio B. Noronha; Production of H_2 from ethanol. Review of reaction mechanism and catalyst deactivation; Chemical Reviews; 112(7), (2012); 4094-4123.
35. Daniel G. Araiza, Antonio Gómez-Cortés, Gabriela Díaz; Effect of ceria morphology on the carbon deposition during steam reforming of ethanol over Ni/CeO_2 catalysts; Catalysis Today; 349 (2020); 235-243
36. Y. Madier, C. Descorme, A.M. Le Govic, and P. Duprez; Oxygen mobility in CeO_2 and $Ce_xZr_{(1-x)}O_2$ compounds: Study by CO transient oxidation and 18O/16O Isotopic exchange; J. Phys. Chem. B; 103,(1999); 10999-11006.
37. Raul Carrera Cerritos, Rosalba Fuentes Ramirez, Alberto F Aguilera Alvarado,J. Merced Martinez Rosales, Tomas Viveros Garcia, Ingacio R. Galindo Esquivel; Steam reforming of ethanol over Ni/Al_2O_3-La_2O_3 catalysts synthesized by sol-gel; Ind. Eng. Chem. Res; 50(5), (2011); 2576-2584.
38. Zenab Abbas, Mythili Surendran, P. A. Anjana, P. K. Jidev, Harshini Dasari, N. Sudhakar Naidu, S. Anandhan, K. Udaya Bhat, G. Uday Bhaskar Babu, Hari Prasad Dasari; Solubility limits of ceria-zirconia-lanthana solid solutions; Materials Today Proceedings; 4(9), (2017); 9360-9364.
39. Matthias Thommes, Katsumi Kaneko, Alexander V. Neimark, James P. Olivier, Francisco Rodrigeuz-Reinoso, JeanRouquerol and Kenneth S. W. Sing; Physisorption of gases, with special reference to the evaluation of surface area and pore size distribution (IUPAC Technical Report); IUPAC Technical report, Pure Applied Chem. 2015.
40. H. Lauron-Pernot, F. Luck and J. M. Popa, Appl. Catal., 78 (1991); 213–225.
41. Seung Ju Han, Yongju Bang, Jeong Gil Seo, Jaekyeong Yoo, In Kyu Song, International Journal of Hydrogen Energy; 38 (2013); 1376-1383.
42. Licheng Liu, Zhen Zhao, Wang Xinping, Hong He; Preparation of ceria-zirconia solid solution with enhanced oxygen storage capacity and redox

performance; Frontiers of Environmental Science & Engineering in China; 4(2), (2010); 164-171.

43. Akihiko Suda, Yoshio Ukyo, Hideo Sobukawa and Masahiro Sugiura; Improvement of Oxygen Storage Capacity of CeO_2-ZrO_2 Solid Solution by Heat Treatment in Reducing Atmosphere; Journal of Ceramic Soc. Of Japan; 110 (1278), (2002); 126-130.
44. Chaunyong Huang, Zilong Tang and Zhongtai Zhang; Differences between Zirconium hydroxide ($Zr(OH)_4.nH_2O$) and hydrous zirconia ($ZrO_2.nH_2O$) Journal of American Ceramic Society; 84(7), (2001); 1637-38.
45. R. Agustín-Panadero, J. L. Román-Rodríguez, A. Ferreiroa, M. F. Solá-Ruíz, A. Fons-Font. Zirconia in fixed prosthesis. A literature review; Journal of Clinical and Experimental Dentistry; 6(1), (2014); 66–73.
46. Hasan Gocmez and Hirotaka Fujimori; Synthesis and characterization of ZrO_2-MgO solid solutions by citrate gel method, Materials Science and Engineering: B; 148 (1-3), (2008); 226-229.
47. Israel Wachs; Infrared spectroscopy of supported metal oxides; Colloids and Surfaces A: Physicochemical and Engineering aspects; 105 (1995); 143-149.
48. H. Knozinger and P. Ratnasamy; Catalytic aluminas surface models and characterization of surface sites; Catal. Rev. Sci. Eng; 17(1), (1978), 31-70.
49. Hongguang Li, Xi Jiao, Lei Li, Ning Zhao, Fukui Xiao, Wei Wei, Yuhan Sun and Bingsheng Zhang; Synthesis of glycerol carbonate by direct carbonylation of glycerol with CO_2 over solid catalysts derived from Zn/Al/La and Zn/Al/La/M (M = Li, Mg, and Zr) hydrotalcite's; Catalysis Science & Technology; 5 (2015); 989-1005.
50. Sonja Kouva, Jenni Andersin, Karoliina Honkala, Juha Lehtonen, Leon Lefferts and Jaana Kanervo; Water and carbon oxides on monoclinic zirconia: experimental and computational insights; Physical Chemistry; 16 (2014); 20650-20664.
51. https://www.clariant.com/en/Corporate/News/2021/11/Clariant-amp-Technip-Energies-launch-EARTHreg-Pioneering-technology-to-reduce-the-CO2-footprint-of-s